Strain partitioning within bending orogens, new insights from the Variscan belt (Chiroulet-Lesponne domes, Pyrenees)

Bryan Cochelin, Baptiste Lemirre, Yoann Denèle, Michel de Saint Blanquat

Strain partitioning within bending orogens, new insights from the Variscan belt (Chiroulet-Lesponne domes, Pyrenees)

Bryan COCHELIN[1,2,3,4]*, Baptiste LEMIRRE[2,5], Yoann DENÈLE[2], Michel DE SAINT BLANQUAT[2]

[1] BRGM DGR/GSO, BP 36009, 45060 Orléans, France

[2] Géosciences Environnement Toulouse, Université de Toulouse, CNRS, IRD, UPS, CNES, 31400 Toulouse, France

[3] Université d'Orléans, CNRS, BRGM, ISTO, UMR 7327, 1A Rue de la Ferollerie, 45071 Orléans, France

[4] State Key Laboratory for Mineral Deposits Research, Nanjing University, Nanjing 210093, China

[5] DREAL Grand Est, SPRNH/PSO/UPC SAMA, 51000 Châlons-en-Champagne, France

Submitted to ***Tectonics***, 17 June 2020

Revised 11 June 2021

* Corresponding author: Bryan Cochelin (bryan.cochelin.get@gmail.com)

Key points:

- The Variscan crust of Pyrenees documents vertical strain partitioning: lateral flow vs upper-crust thickening in the core of Pangea

- We document horizontal strain partitioning between extensional and compressional domains during plate-scale oroclinal bending

- Large-scale strain patterns of bending hot orogens reflect initial conditions (at the onset of bending) and evolving free-boundaries

Abstract

This study investigates how strain is partitioned within hot orogenic belts in a context of plate-reorganization. We document crustal-scale strike-slip shear zones, plate-scale oroclinal bending, and widespread exhumation of deep crustal domains in the core of nascent Pangea plate during late-Variscan times (ca. 310-290 Ma). The role of strain partitioning in the finite strain patterns is first highlighted at regional-scale by a new detailed structural, kinematic, and petrologic analysis of the Chiroulet and Lesponne gneiss domes in the Pyrenees. Vertical strain partitioning in response to N-S shortening-dominated dextral transpression is secondly documented at the scale of the Variscan domains of the Pyrenees, based on a synthesis of recent geochronological, thermobarometrical, and structural data. We show that the mid-lower crust is affected by eastward lateral flow and the upper crust by penetrative thickening and localized thrusting. Local transverse extension in the mid-lower crust illustrates gravity-driven instability favored by the accumulation of anatectic melts in gneiss domes. Finally, we highlight the respective position of extended and shortened area within the Variscan belt during late-Carboniferous/early-Permian that suggests large-scale lateral strain partitioning and reorganization of the weak continental crust in the core of the Pangea. This distribution appears significantly different from other orogens in a similar context of oroclinal bending, resulting in localization of the shortened zones in the core of the belt. This highlights the influence of the initial and boundary conditions, such as the obliquity of the belt to the applied stress field and the location of free-boundaries, on finite strain patterns.

1. Introduction

The understanding of how convergence is accommodated by the lithosphere remains an important issue in tectonics, for both recent and old orogenic belts (e.g., Conand et al., 2020; Torvela & Kurhila 2020). Mass transfer within a crust subjected to convergence can be variably accommodated, depending on the rheological behavior of the colliding lithospheres (e.g., Davy, 1986, Brun, 2002). Under abnormally hot thermal conditions, the weak orogenic crust is subjected to crustal flow and heterogeneous accommodation of strain, which is strongly partitioned (Davy & Cobbold, 1991; Gapais et al., 2009; Chardon et al., 2009; 2011). Strain can be partitioned vertically, combining lateral horizontal flow (i.e., escape) within the weak lower crust and thrusting along the direction of shortening within the upper crust (Cagnard et al., 2006; Chardon et al., 2009; Bajolet et al., 2015). In such a context, the weak and buoyant lower crust can be exhumed up to shallow levels in response to gravity instability, leading to the formation of syn-convergence gneiss domes (Teyssier & Whitney, 2002; Yin, 2004; Whitney et al., 2004; Cagnard et al., 2007; Chardon et al., 2009). Strain can also be partitioned laterally, leading to the coeval development of thrust, strike-slip, and extensional zones through orogens (Teyssier & Whitney, 2002; Tikoff et al., 2004). Both vertical and horizontal strain partitioning are significantly enhanced in a context of orocline formation (Bajolet et al., 2013; Johnston et al., 2013; Krýza et al., 2019). The Himalayan-Tibet orogenic system, bordered by the Pamir-Punjab and the Namche Barwa syntaxes at its western and eastern edges, respectively, fully illustrates the impact of both lateral and vertical strain partitioning in hot orogens. Indeed, strain is accommodated by thrusting at the front of the belt while the ductile crust from the orogenic plateau is extruded laterally and transversally, exhuming deep crustal rocks within gneiss domes along with the Himalayan ranges (Tapponnier et al., 1982; Gapais et al., 1992; Clark & Royden,

2000; Stephenson et al., 2001; Beaumont et al., 2001; Taylor & Yin, 2009). Lateral-escape accommodation by wrenching is well-expressed at the edges of the belt, and especially in response to the development of orogenic syntaxes (e.g., Searle 1996; Bosboom, et al., 2014; Bajolet et al., 2015). As noticed by several authors, the Himalayan-Tibet system shares similar structural patterns with the Variscan belt of Western Europe (e.g., Matte 1991, Vanderhaeghe & Teyssier, 2001). Indeed, the Variscan belt was characterized by coeval development of crustal-scale, strike-slip shear zones (Fig. 1, e.g., Arthaud & Matte, 1975; Matte, 2001; Carreras & Druguet, 2014; Díez Fernández & Pereira, 2017), plate-scale oroclinal bending (Fig. 1, e.g., Gutiérrez-Alonso et al., 2004; Weil et al., 2010) and widespread exhumation of deep crustal domains (e.g., Burg et al., 1994; Martínez Catalán et al., 2007; Gapais et al., 2015; Authemayou et al., 2019). While most of the tectonic models focused on strain partitioning within the collapsing hinterland, only a little attention was paid to strain patterns from the foreland of the belt and the link between them was poorly investigated. But both the hinterland and the southern foreland of the Variscan belt were affected by a diffuse and late reorganization of early orogenic structures during the late-Carboniferous to the early-Permian period (310-290 Ma). It is associated with high-to ultra-high temperature metamorphism (Pin and Vielzeuf, 1983; Barbey et al., 2015; Kunz et al., 2018), and bi-modal magmatism that has affected the whole southern part of the Variscan belt (Martínez Catalán et al., 2014; Moyen et al., 2017; Petri et al., 2017; Lemirre et al., 2019). The widespread high-temperature event suggests lithospheric-scale thermal anomaly associated with the removal of the lithospheric root (Gutiérrez-Alonso et al., 2004; Buzzi & Gaggero, 2008; Laurent et al., 2017). The southern foreland of the Variscan belt centered on the Cantabrian orocline and the Variscan domain from the Pyrenees were also affected by this thermal anomaly despite these domains did not suffer significant thickening before the high-

temperature deformation event (de Saint Blanquat et al., 1990; Weil et al., 2013; Cochelin et al., 2017).

In this context, the common history of the Cantabrian orocline and the Variscan domains of the Pyrenees during late-Variscan evolution remains a significant issue to understand late mountain range evolution and crust-mantle interactions. The Cantabrian orocline located at the core of the Iberian Armorican arc (Fig. 1), is associated with about 180° of cumulative vertical rotation (clockwise and counter-clockwise for the northern and the southern limbs, respectively) of early orogenic structures (Weil et al., 2013; and references therein) between 305 and 295 Ma (Weil, 2006; Weil et al., 2010). Two typical strain patterns were recognized around this late-orogenic structure, depending on their position within or at the limbs of the arc. The core of the arc (i.e., the Cantabrian Zone) is characterized by contractional structures, such as arc-radial folds and steep E-W striking thrusts (e.g., Pérez-Estaún et al., 1988; Bahamonde et al., 2007; Merino-Tomé et al., 2009; Pastor-Galán et al., 2014; Blanco-Ferrera et al., 2017; García-López et al., 2018, Fig. 1). To the contrary, the branches of the arc (e.g., Armorican massif, Central Iberian Zone) exhibit arc-parallel stretching, accommodated by both lateral wrenching and extension (e.g., Martínez Catalán et al., 2007; Gapais et al., 2015; Díez Fernández & Pereira, 2017; Authemayou et al., 2019). Based on this apparent opposition, it has been proposed that the cause of oroclinal bending is an active buckling at lithospheric-scale that was responsible for contrasted mass transfers in the arc, depending on the relative position in the inner and outer arc (Gutiérrez-Alonso et al., 2012). However, compressive/transpressive tectonics is not restricted to the core of the Cantabrian orocline but seems to had developed coevally in the rest of the southern Variscan belt (i.e., the Gondwanan margin), such as the Alpine External Crystalline Massifs (Fréville et al., 2018), the Maures-Tanneron and Corsica-Sardinia massifs (Rolland et al., 2009; Casini et al., 2015), the

Meseta (Alleghenian belt, Michard et al., 2010; Delchini et al., 2018) and the Axial Zone of the Pyrenees (Cochelin et al., 2017) (Fig. 1).

The Variscan domains of the Pyrenees provide excellent markers to study the influence of combined lateral and vertical strain partitioning during structural plate reorganization that led to oroclinal bending. These domains consist of a late-Variscan (i.e., 310-290 Ma) transpressive segment that corresponds to the so-called Pyrenean Axial Zone and sparse massifs under Mesozoic cover to the North, the North Pyrenean massifs (NPM) (Fig. 2a). The lower crust was affected by lateral horizontal flow while the upper crust was strongly squeezed and affected by thrusting along the direction of shortening (Cochelin et al., 2017; 2018a). This structural pattern highlights a very peculiar crustal-scale type of deformation in the foreland of the Variscan belt during its late structural reorganization.

This paper aims to clarify the role of multi-scale strain partitioning in the tectonic evolution of orogenic belts subjected to a structural late-reorganization and bending by focusing on the southern part of the Variscan belt, which is located in the core of Pangea during the late-Carboniferous to early-Permian period. To address this issue, we illustrate how vertical strain partitioning controlled gneiss dome formation in the Pyrenees by providing a new structural, kinematics, and petrological study on the Chiroulet and Lesponne massifs, located at the north-western corner of the Axial Zone (Fig. 2a). Coupled with a synthesis of published structural, geochronological, and metamorphic data from the whole Variscan domains of the Pyrenees (Figs. 2b & 2c), these data are integrated at the scale of the southwestern Variscan belt. We highlight how the interaction between localization of mantle heat source and large-scale vertical and lateral strain partitioning led to the coexistence of strike-slip, compressional/transpressional, and extensional/transtensional tectonic belts. By comparing the Variscan belt of Western Europe with

136 the west Himalayan syntax, we discuss the influence of initial and boundary conditions and
137 thermal states of the colliding lithospheres on finite strain patterns in a context of lithosphere
138 bending.

139 **2. Geological setting**

140 2.1 The Variscan domains of the Pyrenees in the Variscan belt

141 The Western Europe massifs (i.e., Armorican Massif, Iberian Massif, French Massif Central,
142 Bohemian massif, Fig 1) recorded a late-Carboniferous to early-Permian orogenic dismantling
143 associated with high-thermal conditions. This plate-scale event took place after a period of
144 amalgamation of a series of micro-plates with Laurussian margin and a major collisional event of
145 these amalgamated continental blocks with the Gondwana land-mass, during Devonian and
146 Carboniferous times (e.g., von Raumer et al., 2013; Edel et al., 2018; Lotout et al., 2020).

147 During the main collision phase in Western Europe massifs, the Variscan domains of the
148 Pyrenees corresponded to the distant foreland of this orogenic system that recorded deep-sea to
149 platform sedimentation at Devonian to mid-Carboniferous times (see García-Sansegundo et al.,
150 2011 and references therein) and ultimately turbiditic deposition (Delvolvé & Perret, 1989).
151 Flysch deposition is associated with an early tectonic phase, called D1, that was locally preserved
152 as a relic in the Axial Zone (Cochelin et al., 2017 and references therein). Where preserved, D1
153 features are characterized in the upper crust by south-westward to westward thrusts and
154 recumbent or overturned folds (Matte, 2002; Cochelin et al., 2017). These structures induce no
155 significant stratigraphic or structural breaks and were interpreted as reflecting thin-skinned
156 tectonics in the distant foreland of the Variscan belt, between 325-310 Ma (Cochelin et al., 2017).
157 Few occurrences of foliation relics were noticed in the mid-to-lower crust but its relation with D1

structures observed in upper crustal levels remains unconstrained (de Hoÿm de Marien et al., 2019). The D1 tectono-metamorphic event in the Pyrenees is poorly recorded, but it is supposed to produce moderate thickening of the crust, as exemplified by preserved occurrences of prograde M1 metamorphism (Barrovian) in the Canigou massif (de Hoÿm de Marien et al., 2019, Fig. 2c). A slight increase of pressure of about 1 kbar, from 5.5 to 6.5 kbar, has been reported by these authors.

Late Variscan deformation under a high-temperature regime is responsible for the strain pattern of the Variscan domains of the Pyrenees. This strain pattern is marked in the Axial Zone by two distinct structural levels, the so-called Superstructure and Infrastructure (De Sitter & Zwart, 1960) that corresponds to the upper and mid-lower crustal levels, respectively. The Superstructure is made of low-grade Paleozoic metasedimentary rocks affected by intense folding (Carreras & Capella, 1994), an associated N100°E-striking steep axial plane cleavage (Fig. 3) bearing vertical stretching lineations and host the large calc-alkaline plutons (Cochelin et al., 2017; 2018a,b). The Infrastructure corresponds to the partially molten mid-lower crust that is observed within longitudinally elongated gneiss domes (Denèle et al., 2007; 2009; Mezger, 2009). These gneiss domes are defined by shallowly dipping foliation planes bearing longitudinal (i.e., parallel to the belt) stretching lineations (Fig. 3; Cochelin et al., 2018a). In details, the Superstructure is characterized by an incomplete fan of schistosity, interrupted by Alpine faults, especially the North Pyrenean Fault (NPF) to the North, with a vertical domain in the northern half part of the Axial Zone and a domain of dip decreasing southward (Zwart, 1979; Cochelin et al., 2018a). Geostatistical analysis of cleavage suggests that the zone affected this fan of schistosity was initially 80-100 km wide (Cochelin et al., 2018a). Furthermore, the northern domain localized near the NPF was mainly affected by apparently intense coaxial (i.e., non-

rotational) deformation while the southern one is characterized by non-coaxial "north side up" (i.e., the northern block goes upward and the southern downward) or "top to the south" shearing. A dextral component of shearing is also observed and appears restricted to the vicinity of plutons and gneiss domes (Cochelin et al., 2018a). Within gneiss domes belonging to the Infrastructure, the direction of stretching tends to evolve vertically from E-W in the core of gneiss domes to oblique or transverse at their roof (Fig. 3). There, strain localization can be observed within the andalusite zone forming retrogressive extensional shear zones (Van den Eeckhout & Zwart, 1988; Mezger & Passchier, 2003; Cochelin et al., 2017; Le Bayon & Cochelin, 2020). The gneiss domes are mostly folded, with folds showing steep or south verging overturned limbs that are partially reworked by steep reverse-dextral shear zones (Carreras et al., 1980; Vilà et al., 2007; Denèle et al., 2007; 2008; 2009). These reverse-dextral shear zones have been developed under amphibolite-to-greenschists facies conditions and defined an anastomosed network that has affected the evolution of gneiss domes (Denèle et al., 2007; Cochelin et al., 2018a) and the dynamics of pluton emplacement (Gleizes et al., 1998; Denèle et al., 2008).

The mode of formation of the Superstructure and the Infrastructure was widely debated since the '60s (e.g., see Carreras & Capella, 1994) but a coeval formation under N-S shortening-dominated transpression, called D2, reached consensus since two decades (e.g., Gleizes et al., 1998; Mezger, 2009; Denèle et al., 2014; Cochelin et al., 2017). Coeval formation of these two structural domains was interpreted as reflecting vertical strain partitioning between a partially molten and hot middle crust and the cold upper crust (Denèle et al., 2007; 2009; Cochelin et al., 2017). It should be noted that this vertical structural zonation was only partially recognized in the NPM. While a transpressional regime was advocated in the Trois-Seigneurs and the Agly massifs (Leblanc et al., 1996; Gleizes et al., 1998; Olivier et al., 2004), the other massifs (Ursuya,

Castillon, St Barthélémy) have been affected by crustal thinning, permitting the exhumation of Low-Pressure granulites thanks to the activation of extensional shear zones/detachments bearing mainly transverse direction of stretching (Fig. 3) (de Saint Blanquat et al., 1990; Cochelin et al., 2017, Saspiturry et al., 2019). In the Agly massif, crustal thinning was described as occurring during dextral transpression (Olivier et al., 2004; Vanardois et al., 2020; Siron et al., 2020).

The late-Carboniferous/early-Permian thermal anomaly is characterized in the Variscan massifs of the Pyrenees by partial melting of the mid-lower crust under Low-Pressure amphibolite facies in the Axial Zone and Low-Pressure granulite facies in the NPM (Vielzeuf, 1984; de Saint Blanquat et al., 1990; Guitard et al., 1996; Vilà et al., 2007; Aguilar et al., 2015, Lemirre, 2018, Figs. 2c, d & e). In details, available PT estimates for peak metamorphism show that apparent metamorphic gradient within the crust of the Pyrenees at ca. 300 Ma can be divided into two parts (Figs. 2d & e), i) a first part showing high metamorphic gradients (i.e., between 55 and 90°C/km) up to ca. 3 kbar and ii) nearly isothermal conditions within the partial molten middle crust. Temperature peak in the middle crust is around 700-750°C within the Axial Zone and 800-850°C within the North Pyrenean Massifs, corresponding to the wet solidus and biotite dehydration melting reaction respectively (Figs. 2d & e). In most of the gneiss domes, exhumation favored by extensional shearing is well imaged by clockwise PT paths (Fig. 2c), implying nearly isothermal decompression (e.g., Roc de France), heating and decompression (e.g., the Bossost dome), or cooling and decompression (the Albères massif, Fig. 2c). Locally, decompression was followed by heating and a slight increase in pressure (e.g., the Canigou and Aston domes, Fig. 2c).

Partial melting in the mid-lower crust is associated with intrusion of numerous large calk-alkaline plutons in the upper crust (i.e., between 2 and 3 kbar, Fig. 2c) and leucogranites or mafic sills in

the middle crust (i.e., for pressure higher than 3 kbar; Debon et al., 1996; Denèle et al., 2014; Kilzi et al., 2016). These calk-alkaline plutons are made of successive intrusion of magmas from gabbroic to granitic compositions having hybrid to mantle sources (Debon et al., 1996; Lemirre et al., 2019). Magmatism mainly took place between 305 and 290 Ma, coevally with the D2 transpressional phase (Denèle et al., 2014; Druguet et al., 2014; Kilzi et al., 2016; Lopez-Sanchez et al., 2018; Lemirre, 2018; Lemirre et al., 2019, Fig. 2b). Magmatism may have started earlier locally (Aguilar et al., 2014; Lopez-Sanchez et al., 2018; Schnapperelle et al., 2020) and continued up to 270 Ma in the Basque and North Pyrenean Massifs (Fig. 2b).

2.2 The Chiroulet and Lesponne domes in the northwestern corner of the Pyrenean Axial Zone

The Chiroulet and the Lesponne massifs correspond to two neighboring gneiss domes, located in the north-western corner of the Axial Zone between the Néouvielle pluton to the south and the NPF to the north (Fig. 3). Forming two 15 km long and 5 km wide elliptical bodies, they represent the smallest gneiss domes of the Axial Zone. The Lesponne dome sensu-lato corresponds to a succession of three sub-domes, the Lesponne sub-dome sensu-stricto, the Aigue-Rouye sub-dome, and the Gripp anticline from west to east, respectively (Fig. 4a). Along with the Bossost dome located in the Central Axial Zone (Fig. 3), the Chiroulet-Lesponne domes are the shallowest of the Axial Zone, as sillimanite and andalusite isograds reached the upper Paleozoic series (Pouget, 1984; Ternet et al., 1996). The case of the Chiroulet massif is unique in the Axial Zone because the anatectic front is located at the transition between Silurian black schists and Devonian limestones while it is located in lower Paleozoic rocks in the other massifs (Guitard et al., 1996 and reference therein). The core of these gneiss domes is composed of metatexites and bimodal plutons (diorites and leucogranites) for the Lesponne dome, and diatexites with

leucogranite sheets for the Chiroulet dome. Metamorphic conditions of partial melting have been estimated at ca. 700 °C and 4.2 kbar in the Lesponne dome (i.e., at mid-crustal depths, see Lemirre et al., 2019, Fig. 2b). Geochemistry shows that the dioritic magma is associated with a mantle source while leucogranites are issue from partial melting of surrounding metasedimentary rocks (Lemirre et al., 2019). In the Lesponne and Chiroulet massifs, partial melting started at ca. 303 Ma and the final crystallization of magmas occurred at ca. 290 Ma, suggesting that the mid-lower crust stayed hot (i.e. around 700°C) and partially molten during 10 My (Lemirre et al., 2019, Fig. 2c). Based on petrostructural studies, Pouget (1984, 1987) and Pouget et al., (1989) have proposed that these massifs form two magmatic diapirs intruding the upper crust in a context of orogenic collision. However, the absence of published mineral-stretching lineation measurements or kinematic data makes it difficult to ascertain the tectonic context of their formation.

3. Methods

This work is based on 197 field stations, where petrographic, structural and kinematic analysis were performed (see Supporting Information). To retrieve how the gneiss domes were emplaced within the upper crust, planar and linear strain fabrics and kinematic criteria were systematically measured. The studied area is characterized by the interference between two regional penetrative fabrics. The first defines the main foliation within migmatites, paragneiss, and sillimanite-andalusite bearing micaschists. The second is an axial plane cleavage, moderately to steeply dipping to the south, mainly observed in upper crustal low-grade rocks. This cleavage is marked by oriented biotites and chlorites. As these two fabrics characterize respectively the Infrastructure (i.e., the middle crust) and the Superstructure (i.e., the upper crust), we call them “Si” and “Ss” respectively, following Cochelin et al., (2017) and consequently, the same terminology will be

used for lineations (Li and Ls). Specific attention was paid to the transition between Si and Ss fabrics and we present hereafter their structural relationship by showing the observed interference patterns. These results allow us to propose a revised and harmonized geological map of the area (see Supporting Information), and a structural map based on the compilation of available data and our measurements (Fig. 4b). Our dataset is also presented in Figure 5. New cross-sections over the two massifs (Fig. 6) and field observations (Figs. 7, 8 & 9) are presented, highlighting structural patterns within the upper and middle crust. Besides, 34 samples were collected within the two gneiss domes and their surrounding metasedimentary rocks. Thin-sections were prepared normal to the schistosity and parallel to the mineral-stretching lineation (XZ planes) for petrographic and microstructural analysis (Fig. 10).

4. Results

From a structural point of view, the studied area is divided into three domains: i) the core of the gneiss domes made of migmatites, plutonic rocks (e.g., leucogranite, diorite), and paragneisses, where only Si is observed; ii) the upper crustal domain, where Ss is the main fabrics; and iii) a transitional zone in-between, that has affected the Devonian rocks belonging to the sillimanite-andalusite zone, where interference patterns between Si and Ss can be found. We present hereafter these three domains from bottom to top.

4.1. The lower domain

The lower domain can be defined under the sillimanite-in isograd where gneissic rocks (metatexites and paragneiss) and micaschists show evidence of plastic deformation of quartz, feldspar, phyllosilicates, and alumina silicates that define the foliation Si and the stretching lineation Li.

The map of foliation trajectories highlights a first-order concentric pattern centered on high-grade rocks that define two gneiss domes with N110° and N130° long axis, for the Lesponne and Chiroulet massif, respectively (Fig. 4). Foliation trajectories in north-south cross-sections (Fig. 6) show that the Lesponne dome is upright and symmetrical while the Chiroulet dome is asymmetrical and inclined, with foliation dominantly dipping to the south. The northern limb of the Chiroulet dome is characterized by S-steeply dipping foliation suggesting a domal shape overturned to the north (Figs 4b & 6). The internal structure of the domes displays second-order sub domes (Fig. 4b) with apexes that correspond to the core of magmatic bodies or diatexites in the Lesponne and Chiroulet domes, respectively (Fig. 4). Magmatic rocks (leucogranites and diorites) and diatexites are characterized by more or less defined magmatic foliation and lineation (Fig. 7a, b & c). Structural concordance between the intrusive contact of diorite-leucogranite plutons with their country-rocks and the foliation Si suggests intrusion as magmatic sills (Figs. 6 & 7a). Moreover, consistency between magmatic mineral lineations within magmatic bodies and stretching lineations within their country-rocks reflects that they were deformed synchronously during magmatic events. Mineral/stretching lineations are defined by elongated quartz aggregates, oriented feldspars, patches of micas (Fig. 7c), or oriented amphiboles (Fig. 7d) and show a consistent N110° trend in the Chiroulet dome and N130° in the Lesponne dome (Fig. 4b). Stretching is associated with strain localization into shallowly dipping C' shear bands with a consistent "top to the west" sense of shear (see Cochelin et al., 2017, Fig. 10c). Injection of magmatic veins is common in these shear bands, suggesting deformation during partial melting. At the boundary between the lower domain and the transitional domain of the Chiroulet dome, stretching lineations turn to N-S (Fig. 4b) and C/S structures (following the definition by Gapais, 1989) can be observed within leucogranitic sills, with "top to the south" kinematics (Fig 6, see

Lemirre et al., 2019). Calc-silicate gneisses at the top of the migmatites are affected by antithetic slip boudinage (i.e., domino-like) compatible with “top to the south” shearing (Fig. 7e).

The microstructural study shows that paragneisses and sillimanite-bearing micaschists of the lower domain from the two domes are characterized by strongly oriented fabrics (Figs. 10b, c & d). The association of deformation bands in quartz grains as well as evidence of dynamic recrystallization controlled by grain boundary migration (Fig. 10b) attest to deformation at high-temperature conditions, i.e. >500°C (Stipp et al., 2002; Fossen and Cavalcante, 2017). In the calc-silicate gneisses at the top of the migmatites, Si foliation is parallel to the transposed bedding defined by the alternation of diopside-epidote-sphene layers and garnet-diopside-sphene layers (Fig. 10d). Garnet-rich layer form boudins and the inter-boudins are mostly filled by quartz or calcite-epidote veins (Fig. 10d). In these veins, quartz grains are also recrystallized by grain boundary migration (Fig. 10d’).

4.2. The transitional domain

This domain affects the upper Paleozoic series. It is distributed in a large region in the Chiroulet dome that corresponds globally to the extension of the andalusite-bearing micaschists and is localized within the Silurian black schists in the Lesponne dome. In the Chiroulet dome, the basal limit of the transitional domain corresponds to the contact between the Silurian black schists turned into paragneisses and the Lower Devonian meta-carbonates, both within the sillimanite zone. The upper part of this domain can reach the Upper Devonian series and the Tourmalet shear zone in the southern part of the massif (Figs 4 & 6).

In the transitional domain, a high-strain fabric is marked by the total transposition of the bedding and the development of a pervasive Si foliation. It is responsible for the boudinage of Devonian

siliciclastic layers within the weak marbles. Li stretching lineation is defined by calcite, pyroxene, or amphibole in marbles and sillimanite, andalusite, feldspar, or quartz in schists and paragneisses.

Foliation trajectories show concentric patterns, surrounding domes' cores (Fig. 4b). These foliation trajectories appear highly disturbed by polyharmonic N100° to N130° trending folds, and specifically in the southern border of the Chiroulet dome (Fig. 4b). First-order folds are kilometer-scale, tight to isoclinal (Fig. 6). They exhibit asymmetrical shapes and are all overturned to the north (Figs 6 & 8a). Similar folds may be recognized from meter to decameter scale (Fig. 8). These numerous folds are responsible for multiple repetitions of the schists-marbles intercalations, which could explain why the sillimanite-andalusite metamorphic zones are thicker where these folds exist (Fig. 6).

Li show extremely variable trends, from roughly N-S to E-W but remain dominantly parallel to the Li of the lower domain (Fig 5). On the field, the stretching lineation appears wrapped into regional to local folds (Fig. 7f), suggesting passive reorientation by folding of the Si fabric. When C' shears are associated with stretching, the relative sense of shear is also variable depending on their location in regional folds (Figs. 4b, 5 & 6).

The intense folding of the Si foliation is associated with the development of an N100-130°E axial plane cleavage (Figs 4b & 6). Within the hinges of folds, it forms a crenulation cleavage Ss (Fig. 7g), which is marked by the crystallization of biotites in andalusite-sillimanite schists. Ss is E-W striking and dips moderately to the south (Fig. 5). Localization of deformation in the flanks of regional folds is recorded by the development of a mylonitic foliation mostly developed within the marbles (Fig. 9a). Strain localization strongly reduced the thickness of marbles while tectonic thickening is currently seen at the hinges (Figs 6 & 8a). Folded boudins are common (Fig. 8b, c,

d), which suggests reworking of Si fabric. This mylonitic foliation Ss in marbles bears an N200° down-dip stretching or striae-lineation Ls (Fig. 5), defined by calcite or quartz ribbons (Fig. 7h). Ls lineations are systematically associated with non-coaxial "top to the north" (i.e., reverse) or "South side up" kinematics (Figs 6, 8a,e, & 9a). North-directed thrusting is in accordance with the regional asymmetry of the sheared folds. Similar deformation can be observed within Silurian black schists at the top of the Lesponne gneiss dome, with strain localization of non-coaxial "top to the north" (i.e., reverse) shearing associated with N-S stretching lineations (Fig. 9b). This mylonitic contact has been locally reworked by post-Variscan faulting (see *section 4.4.2* below). At the top of the transitional zone, the Si fabric appears mostly reworked by the steep and penetrative Ss cleavage, with locally few preserved andalusite porphyroclasts. Stretching lineations are still down-dip and kinematics associated with shear bands seems to be mostly reverse (Figs. 4b & 6).

The microstructural study within the limbs of the tight to isoclinal regional folds shows the reworking of the high-temperature Si foliation by Ss mylonitic bands (Fig. 10e, e'). Core and mantle textures characterized the Ss planes (Fig. 10e) with quartz 1 ribbons and a fine-grained matrix of quartz 2 and muscovite forming the core and the mantle, respectively. Undulose extinction and deformation bands in quartz ribbons, as well as the presence of fine quartz grains, underline deformation at middle-temperature conditions probably around 400-450°C, close to the bulging/subgrain rotation transition defined by Stipp et al. (2002).

Near the boundary with the upper domain, chiastolitic-andalusites are partially retrogressed into white micas while biotites are retrogressed into chlorites (Fig. 10f). Chlorite is also formed in pressure shadows of andalusite porphyroclasts (Fig. 10f, f'). Andalusites show inclusions of an early fabric that could be related to peak metamorphism (i.e., Si foliation) (Fig. 10f'). Quartz

grains document evidence of subgrain rotation recrystallization, with quartz blasts of about 20-50 μm (Fig. 10f''), suggesting that deformation occurred at a temperature around 400-500°C (Stipp et al., 2002). The retrogression of biotite, andalusite, and subgrain rotation recrystallization of quartz suggest that reworking of Si by Ss is associated with regional cooling from amphibolite to greenschist facies conditions. These observations are in accordance with estimates at 580°C/2.3 kbar by Pouget (1989) for the peak of metamorphism associated with Si in the transitional domain.

4.3. The upper domain

This upper domain belongs to the biotite and chlorite zones, where the original bedding of the upper Paleozoic series is mainly preserved. These metasedimentary rocks are affected by tight E-W to NW-SE trending folds and a steep axial plane cleavage (Fig. 6). Ss trajectories are molding the gneiss domes, forming neutral points that are preserved at their western parts (Fig. 4b). Locally, strain seems to be localized within Devonian marbles or Silurian black shales, where bedding is transposed. These high-strain zones delineate the longitudinal regional shear zones observed outside of the metamorphic aureoles of gneiss domes (Figs. 3 & 4, e.g., the lateral continuity of the Tourmalet shear zone). The stretching lineations Ls lying on the Ss fabrics have an N200° trend, which is parallel to the Ls measurement within the transitional domain (Fig. 5). Ls is mostly defined by quartz aggregates, calcite ribbons, or white micas flakes. Sense of shear associated with shear planes depends on the dip direction of the shear planes and Ss, showing systematically reverse kinematics (Figs. 5 & 9b). The transition between the two directions of thrusting seems to coincide with the Tourmalet shear zone, with the first occurrences of south-verging thrusts and north-dipping Ss cleavage that are well known in the rest of the Axial Zone (Figs 4b & 6, cross-section 1).

The microstructural study of the Upper Carboniferous sandstones (Fig. 10a) evidences a well-defined cleavage Ss, marked by dissolution joints (Fig. 10g). The matrix is made of very fine grains of quartz, muscovite, and chlorite. Detrital quartz grains are poorly or not recrystallized, showing undulose extinction while quartz from the matrix form aggregates of small crystals showing homogeneous grain size probably developped by bulging recrystallization (Fig. 10g'). It suggests that deformation occurred at temperatures below 400°C (Stipp et al., 2002), in agreement with estimates from Pouget (1989) (400-220°C/2.3 kbar) for the peak metamorphism. The detrital quartz grains show symmetrical patterns, which indicates that deformation was mainly coaxial.

4.4 Early and late deformations:

4.4.1. Early (D1) deformation

In the studied area, occurrences of early deformation can be deduced at a map-scale in the upper domain (Fig. 4). Indeed, moderate overprint of Ss on bedding allows preserving early D1 folds, highlighted by intercalated limestones within Devonian schists (Fig. 4). These pre-Ss folds were variably rotated, showing N-S to ENE-WSW trends outside and near gneiss dome, respectively. Regarding the E-W cross-section (Fig. 6, cross-section 3), it appears that the dome shape of the Lesponne is oblique to regional structures as the gneiss dome was emplaced into Cambro-Ordovician rocks at the east and lower Devonian series at its western termination. This suggests regional west-verging overturned or recumbent folds, like those observed in the western part of the Axial Zone (Matte, 2002; Cochelin et al., 2017). In our studied area, the characteristics of the D1 deformation event are difficult to determine at the scale of the outcrops and no proofs of the existence of an early cleavage S1 have been underlined in the field.

4.4.2. Late and post-Variscan deformation

The magmatic rocks belonging to the lower domain were affected by localized low-grade (i.e. chlorite stability field) ductile deformation (Fig. 4). It forms E-W to NW-SE meter-scale mylonitic corridors that have been precisely mapped by Pouget (1984), showing an anastomosed pattern. These corridors are steeply dipping and induce local perturbations of Si trajectories (Fig. 4b). As described by Pouget (1984), mylonites are marked by small porphyroclasts of quartz and feldspars and by crystallization of white mica, chlorite, or epidote. The foliation mostly hosts a shallow- dipping stretching lineation, defined by quartz aggregates. Steep C' shears show dextral kinematics (Fig. 9c), which is consistent with the local inflection of Si trajectories (Fig. 4b). A minor vertical component of movement is inferred because of shallowly plunging (i.e. with a pitch between 5 to 45°) stretching lineations. The main low-grade dextral shear zone corresponds to the Chiroulet shear zone, putting diatexites of the northern part of the Chiroulet massif in contact with lower Devonian rocks or small sheets of Silurian black schists belonging to the andalusite zone (Fig. 6). Following Pouget, (1984), these ductile shear zones could also affect the upper domain laterally and are collinear to the regional Ss fabric. Therefore, these shear zones could be Late Variscan in age, like those described in *section 4.3*.

In our studied area, late brittle deformation can be frequently observed and may be related to the Alpine orogeny. The frequency of faults increases towards the north (i.e., towards the NPF, see Fig. 4). They often reactivate Variscan structures such as Ss cleavage or Si foliation plane, with down-dip striation covering the foliations planes with HT paragenesis (e.g., sillimanite, andalusite, biotite, see Fig. 9d & d'). When structural markers are present, such as post-Variscan dykes (Fig. 9d), the faults show reverse sense of shear. Most of the time, Silurian black schists localized faulting, especially around the Lesponne massif. Unfortunately, the amount of

displacement along these faults during Alpine orogeny remains difficult to estimate, as the current position of rocks results from both Variscan and Alpine tectonics. Furthermore, few contacts such as the Oussouet-Cap de la Taoula thrust, seem to have experienced a more complex history, including Post-Variscan normal faulting that could be Permian or Cretaceous in age. Indeed, the reverse movement along the thrust was not sufficient to balance earlier normal faulting (Fig. 6, compare cross-sections 4 & 5). Despite reactivation of Variscan structures, the impact of Alpine faulting remains limited as it doesn't disturb the metamorphic aureoles of gneiss domes (e.g., the andalusite zone of the Lesponne dome stays centered on the sillimanite zone, Fig. 4). Tilting to the north of Variscan structures can be observed at the vicinity of the NPF like in the rest of the Axial Zone (see Cochelin et al., 2017) but this effect vanished 1-2 km south of the fault (Ternet et al., 1996). The structural and metamorphic continuity and the absence of large block rotation are thus well presented in our cross-sections (Fig. 6).

5. Discussion

5.1. Gneiss dome formation by vertical strain partitioning

Based on our structural and microstructural observations, and the integration of petrological and geochronological data, we propose a scenario in which the Chiroulet-Lesponne gneiss domes were formed in two steps during the D2 tectonic phase (Fig. 11). The two steps, that follow up an early folding event in the upper crust (D1 phase Fig. 11a), have occurred in a continuum during progressive cooling of the crust, subsequent to peak metamorphism and partial melting.

5.1.1. Initiation of gneiss dome formation during longitudinal mid-crustal flow

Deformation at peak metamorphic conditions is marked by strain partitioning between the upper crust and the partially molten middle crust. The metasedimentary rocks of the upper crust were

476 subjected to vertical stretching, folding, and formation of a steep axial plane cleavage. Syn-
477 kinematic plutons such as the Néouvielle pluton to the South of the Chiroulet dome were
478 emplaced in the upper crust and were affected by a weak deformation at sub-solidus to HT solid-
479 state conditions (Gleizes et al., 2001). This deformation, already described in the Axial Zone to
480 the East of the Chiroulet-Lesponne area, is compatible with N-S shortening-dominated
481 transpression and probably occurred from 310 to 300 Ma, during the main phase of pluton
482 emplacement.

483 The mid-lower crust recorded orogen-parallel flow (i.e. longitudinal) and formation of gneiss
484 domes (Fig. 11b). Gneiss dome formation suggests both gravitational instabilities linked to the
485 presence of partially molten rocks and strain localization that induced local upward flow.
486 Exhumation of gneiss core is marked by an isothermal decompression path in the migmatites, up
487 to ca. 3 kbar while the transitional domain recorded only a minor decrease of temperature (Fig.
488 11b). The impact of strain localization is identified by the contrasted evolution of the Chiroulet
489 and Lesponne domes. The Lesponne dome is in fact, only affected by lateral flow while the
490 Chiroulet dome is marked by the development of a transverse extensional shear zone on the
491 whole pile of Devonian metasedimentary rocks (Fig. 11b). This contrasted style of evolution is
492 correlated with various metamorphic conditions in the Devonian series of the two domes. This
493 suggests an upward propagation of the thermal anomaly in an already structured crust, inherited
494 from the D1 phase (Fig. 11a). The local weakening of Devonian marbles explains the formation
495 of a kilometer-scale decollement level above the migmatites of the nascent Chiroulet dome (Fig.
496 11a, b). Similarly, local orogen-normal extension assisted by strain localization within marbles
497 was also recognized in the Bossost dome located few kilometers to the east (Mezger & Passchier
498 2003; Cochelin et al., 2017) or in the Canigou dome (Le Bayon & Cochelin, 2020).

This event recorded in the Chiroulet-Lesponne area expresses a turning-point of tectonic settings and style of deformation. This turning-point has already been described in the Central and Eastern domains of the Axial Zone synchronously with the widespread metamorphism and magmatism taking place at ca. 310-290 Ma (e.g., Denèle et al., 2014; Lemirre et al., 2019, Fig. 2b). The upward migration of the anatectic front progressively increased the geothermal gradient in the above crust and led to a near isothermal gradient below (Lemirre, 2018; Lemirre et al., 2019). The persistence of this HT geothermal gradient during at least 10 Ma (Lemirre et al., 2019, Fig. 2b) produced a long-lasting weakening of the crust.

5.1.2. Dome amplification and strain localization

Cross-cutting relationships of Ss and Si in the transitional domain, the late formation of north-verging folds and thrusts surrounding the Chiroulet dome, and the formation of chlorite-bearing shear zones that crosscut both the lower and upper crustal domains suggest a continuum of D2 deformation during progressive cooling of the crust, after the peak of the thermal anomaly (Fig. 11c). Progressive cooling of the crust is attested in a significant way by the reworking of the HT Si fabrics by the MT Ss fabrics in the transitional zone. Crystallization of migmatites at ca. 290 Ma (Lemirre et al., 2019) at the top of the gneiss domes seems to constrain the ultimate age of this event. We propose that this period is characterized by a progressive coupling between the transitional domain at the top of the mid-lower crust and the upper crust implying competition between orogen-parallel horizontal flow within the mid-lower crust and vertical stretching in the upper crust. In this context of cooling, the still weak marbles and micaschists surrounding the Chiroulet dome localized compressional deformation, forming north-verging folds and thrusts (Figs. 6 & 11c), and the domal shapes were amplified by large scale folding (Fig. 11c). In the Lesponne dome, the Silurian black schists localized the deformation, preserving the dome from

intense overprint by Ss structures (Fig. 11c). Progressive strain localization within steep retrogressive shear zones at the limbs of gneiss domes allowed overturning the northern flank of the Chiroulet dome (Fig. 11c). These late-Variscan shear zones are well-known in the Axial Zone (e.g., Carreras, 2001, Druguet, 2001; Denèle et al., 2008; Cochelin et al., 2018b) and their activation was recently constrained using U/Pb dating on apatites at ca. 289 Ma in the Central Pyrenees (Poitrenaud, 2018; Poitrenaud et al., 2020).

5.2. Impact of strain partitioning on final strain patterns in orogens

5.2.1. Lateral and vertical strain partitioning within the Variscan crust of the Pyrenees

Structural studies performed at the local scale in the Axial Zone led some authors to the conclusion that only south-directed thrusts can be observed (e.g., García-Sansegundo et al., 2011). This interpretation is due to the truncation of the northern part of the Axial Zone by Alpine structures oblique to Variscan ones, especially in its eastern half part (Fig. 3). Our study in the Chiroulet-Lesponne area, where north-dipping thrusts are preserved, allows us to give a more complete view of the Axial Zone. For these reasons we propose in our conceptual model (Fig. 12a) that the Variscan Axial Zone corresponds to a doubly verging accretionary domain (i.e., a narrow orogenic belt) showing south verging thrusts in the southern part, a highly shortened central domain with apparently coaxial deformation and north-verging thrusts on the northern domain. The layered Variscan crust of the Pyrenees is thus characterized by opposite direction of extrusion in response to N-S horizontal shortening. While mid-lower crust laterally flows (lateral escape), the thickening upper crust is affected by vertical (orogen-normal) extrusion (Fig. 12a). The gneiss dome formation is linked to gravitational instabilities within the partially molten mid-lower crust and strain localization that induced the activation of decollement levels, those latter permitting partial decoupling between the two structural domains. The cooling of the crust at ca.

300-290 Ma induced progressive coupling between the two structural domains, as highlighted by the overprint of retrogressive reverse shear zones on high-grade fabrics within gneiss domes (Figs 11 & 12a). In our model, syn-convergence late-Carboniferous/early-Permian volcano-clastic sediments (i.e., the "grey unit" and "transitional unit", see Pereira et al., 2014) are accumulated into narrow longitudinal basins at the front of these steep thrusts (Fig. 12a) as suggested by recent studies (e.g., Gretter et al., 2015; Lloret et al., 2018). Similar deposition of continental detrital sediments at the front of Gzhelian thrusts was recorded in the Cantabrian Zone (e.g., Pérez-Estaún et al., 1988; Alonso et al., 2009). The transition from deep-sea to intra-continental sedimentation during the Carboniferous-Permian transition also suggests an increasing topography. Thus, the short-lived lateral escape of the mid-lower crust may have not been sufficient to balance overall thickening, which is typical of hot orogen deformation mode (Cagnard et al., 2006; Gapais et al., 2009; Chardon et al., 2009; Bajolet et al., 2015).

In the North Pyrenean Massifs, the deformation appears more heterogeneous than in the Axial Zone with evidence of longitudinal and transverse extension leading to significant crustal thinning and exhumation of the lower crust by the activation of detachment faults (de Saint Blanquat et al., 1990; de Saint Blanquat 1993; Saspiturry et al., 2019). To explain coeval development of extensional structures in the NPM and contractional ones, mostly in the Axial Zone, some advocated the existence of a Late-Variscan NPF separating these massifs (e.g., Arthaud & Matte, 1975; Burg et al., 1994; Matte 2001; Carreras & Druguet, 2014). Following these authors, this supposed - but never observed - lithospheric structure would act as a dextral mega shear zone or a transfer zone. Despite some uncertainties concerning the movement of the Iberian plate at Mesozoic times, a large displacement along the NPF is now widely challenged for the Alpine cycle (Jammes et al., 2009; Tugend et al., 2014, Canérot, 2016; Nirrengarten et al.,

2018, Saspiturry et al., 2019, among others). Therefore, the NPM can be also reasonably considered as the northern continuity of the Axial Zone at Late Variscan times and as a part of the same late-Variscan transpressional tectonic system. In this context, considering that transverse-dominated extension is recorded in the massifs marked by granulite facies metamorphism (e.g., Agly, St-Barthélémy, Castillon, Ursuya, Fig. 3) and that the other massifs recorded only amphibolite facies metamorphism, we suggest that transverse extension is driven by local drastic rheological weakening of the crust. The contrasted structural patterns of the Axial Zone and the North-Pyrenean massifs can be interpreted in terms of lateral strain partitioning due to rheological heterogeneities within the abnormally hot crust during the late-Carboniferous to early-Permian period.

5.2.2. Towards an integrated view of continental mass transfers in the southwestern Variscan realm during Pangea amalgamation

In the Variscan domain of the Pyrenees, vertical strain partitioning occurred between 310 and 290 Ma (e.g., Denèle et al., 2014; Lemirre et al., 2019; Poitrenaud et al., 2020, Fig. 2b) synchronously with large mass transfers that affected the ongoing dismantling Variscan belt under abnormally hot thermal conditions (Fig. 12b). During this short period, folding of the whole Variscan belt led ultimately to the closure of the Iberian-Armorican arc (Cochelin et al., 2017) and the formation of the Cantabrian Orocline (e.g., Weil et al., 2010; Edel et al., 2018). Following the model of formation of the Cantabrian Orocline by bucking of the lithosphere by Gutiérrez-Alonso et al., (2004), shortened areas are supposed to be restricted to the inner parts of the arc (i.e., the Cantabrian Zone) while the outer arc was subjected to widespread extension or wrenching. This model explains lateral strain partitioning in NW Iberia but fails to explain why compression/transpression occurred coevally in many places in the southern realm of the

Variscan belt (see the introduction, Fig. 1). We propose that occurrences of transpressive restraining bends in the southern Variscan belt at the late-Carboniferous to early-Permian period reflect lateral strain partitioning and global reorganization of weak continental masses following the ultimate accretion of Gondwana and Laurentia (Fig. 11b). Indeed, the persistence of high geotherms in the Variscan belt (e.g., Fig. 2d, e) due to widespread partial melting and accumulation of magmas in the middle crust after lithospheric delamination (Gutiérrez-Alonso et al., 2004; Buzzi & Gaggero, 2008; Laurent et al., 2017), as exemplified in most of the massifs (Fig. 11b), favored global strain partitioning and triggered extreme mobility of the continental crust. In such a model, three end-members are exemplified (Fig. 12), reflecting how strain can be partitioned within the orogen: i) transpressive restraining bends (Variscan crust of the Pyrenees; Fig. 12a) ii) domains affected by lateral escape combining wrenching and lateral extension (Armorican Massif; Fig. 12c), and iii) those affected by transverse extension and gravitational collapse, (East Massif Central; Fig. 12d). Coeval generation of folds and steep thrusts showing E-W trends in the Cantabrian Zone and the Axial Zone in response to N-S shortening (in present coordinates) in Iberia implies that these two massifs could have formed a single and continuous transpressional restraining bend. The Cantabrian-Axial Zone restraining bend could extend eastward in a Gondwananan autochtonous domain that could correspond to the Mycenian domain belonging to the Paleotethys realm (Stampfli et al., 2013) but such a hypothesis remains uncertain because of the dismembering of the Iberian plate at Cenozoic times (Jolivet et al., 2020). At least two other restraining bends were formed at the Carboniferous-Permian boundary, both southwestward (the Alleghanian belt) and northeastward (Maures – Sardinia – Alpine External Crystalline Massifs) (Fig. 12b). Therefore, it appears that shortening was not only accommodated around bending oroclines as expected by Pastor-Galán et al., (2018) but at a larger scale, within

614 the entire core of the Pangea supercontinent, coupling lateral extension, wrenching (Fig. 12c),
615 and the formation of highly shortened domains (Fig. 12a, b).

616 *5.2.3. Strain patterns in hot bending orogenic belts and their link to geodynamic evolution*

617 The Western arcuate Variscan belt has been compared to the Pamir West Himalayan syntax
618 (Matte, 1986; 1991). Since oroclinal bending appears to occur in a very different way as the
619 Indian Craton indenter have no equivalent in the weak late-Variscan domain squeezed between
620 the Laurussia and Gondwana cratonic land-masses (Fig. 13), these two belts are indeed
621 characterized by (i) development of crustal-scale strike-slip shear zones on the two branches of a
622 nascent syntax (e.g., Martínez Catalán, 2011; Zhang & Sun, 2020), (ii) strain partitioning
623 processes leading to the exhumation of the deep crustal rock within extensional gneiss domes and
624 syn-convergence lateral and transverse escape of the weak mid-lower crust (Gapais et al., 1992;
625 Stephenson et al., 2001; Martínez Catalán et al., 2014; Gapais et al., 2015; Rutte et al., 2017), (iii)
626 accommodation of deformation over large distances (i.e. more than 600 km wide orogenic belts)
627 in a hot and weak orogenic lithosphere bounded by strong and colder cratonic lithospheres (Fig.
628 13).

629 However, the spatial distribution of domains affected by lateral escape, transverse extension, and
630 compression differs in many ways. Above all, it should be noticed that NNE-SSW convergence
631 at ca. 300-290 Ma in the Variscan belt is mostly due to an intracontinental collision (i.e., intra-
632 Pangea) that led to the formation of the Alleghanian belt (Michard et al., 2010; Edel et al., 2018;
633 Figs. 1 & 12b), to the south-west of Western Europe. Thus, the structures that were formed at this
634 period result from the roughly northeastward propagation of stress within the initially NE-SW-
635 trending Variscan belt (Edel et al., 2018 and reference therein). Strain was thus accommodated
636 within a weak lithosphere by bending oroclines, lateral escape, and the formation of

637 compressional/transpressional domains, which are distributed as restraining bends within the
638 whole southern part of the Variscan belt (Fig. 13a). On the contrary, the domains subjected to
639 compression appear as restricted to the edge of the orogen in the Himalayan-Tibet system (Fig.
640 13b). This difference may be explained by the fact that the Variscan belt was affected at ca. 310-
641 300 Ma by orogen-parallel stress (Johnston et al., 2013, Edel et al., 2018) while the Himalayan-
642 Tibet system only recorded orogen-perpendicular stress (e.g., Bosboom, et al., 2014).

643 Syn-convergence gneiss dome formation by transverse extension is common in the Pamir syntax
644 (Fig. 13b), reflecting gravity-driven instabilities within the orogenic plateau (Rutte et al., 2017;
645 Worthington et al., 2020), which may be favored by decoupling between the lower and the upper
646 plate (Bajolet et al., 2015). On the contrary, gneiss dome formation by transverse extension at ca.
647 300 Ma remains rare in the Variscan belt, and occurrences are restricted to the Eastern Massif
648 Central, or, as described in this study, in few NPM. While those from the NPM are similar to the
649 gneiss domes that were developed in the Pamir syntax (i.e., syn-convergence), those from the
650 eastern Massif Central look different. Indeed, this massif only recorded N-S extension at 305-300
651 Ma, leading to the development of widespread sedimentary basins and locally extensional domes
652 (Fig. 13a) (Faure et al., 2009; Ducassou et al., 2019; Vanderhaeghe et al., 2020 and references
653 therein). This suggests a regional evolution with its own dynamics in response to an asymmetric
654 delamination process (Laurent et al., 2017). There, N-S extension could also reflect the influence
655 of the Paleothethys realm to the south (Fig. 12a), which corresponds to a geodynamic free edge.
656 Indeed, roughly N-S extension was recorded within the Paleotethys realm since ca. 300-290 Ma
657 (e.g., Angì et al., 2010; Edel et al., 2014 and references therein). In our model of continuous
658 Cantabrian-Axial Zone restraining bend, longitudinal stretching of the weak lower crust by
659 eastward flow combined to the dextral component of shearing in the upper crust can also reflect

660 the presence of this free edge to the east (Fig. 12a). Similarly, the propagation of the orogenic
661 front and the orogenic plateau to the west in the Himalayan-Tibet system is controlled by
662 boundary conditions. Indeed, the weak plateau involved in the Pamir syntax is extruded westward
663 as squeezed between the Tian Shan block and the Indian craton (Rutte et al., 2017; Worthington
664 et al., 2020).

665 To resume, despite both the Variscan and Himalaya-Tibet orogenic systems corresponds to weak
666 domains subjected to bending during ongoing convergence between strong cratonic blocks, they
667 document contrasted finite strain patterns. Specific strain pattern of bending orogenic system in
668 these two domains seems to be related at first-order to initial boundary conditions at the onset of
669 bending such as the direction of stress vs the trend of the earlier belt, the land-mass vs indenter
670 geometry of cratonic lithosphere, and the evolution of free-boundaries. Concerning the southern
671 Variscan belt, it appears that the marked change in the regional stress direction that has occurred
672 at about 310-300 Ma (Edel et al., 2018) was the expression of the self-subduction of the Pangea
673 that led ultimately to its break-up in Permian times (Gutiérrez-Alonso et al., 2008).

674 **Conclusion**

675 The structural patterns observed in the Chiroulet and the Lesponne gneiss domes illustrate how
676 strain was vertically partitioned within a weak layered crust subjected to shortening. This gave
677 rise to first-order structural constraints to retrieve the tectonic and rheological evolution of this
678 part of the Axial Zone in a context of widespread mass transfers and oroclinal bending in the core
679 of the Pangea.

680 Subjected to a thermal anomaly from the mantle, the lower crust of the Variscan belt was
681 progressively affected by partial melting at ca. 310 Ma. Upward propagation of HT

682 metamorphism induced critical weakening of the crust that was subjected to N-S horizontal
683 shortening. The partially molten mid-lower crust was thus affected by horizontal longitudinal -
684 here eastward - flowing while the upper crust was affected by folding and thickened. Migmatites
685 were partially exhumed due to gravity instabilities, leading to the formation of gneiss domes by
686 extension at their roof. This process was enhanced by the activation of a decollement level
687 located within the kilometer-thick upper Paleozoic marbles. The gneiss domes were then
688 amplified by folding while strain was localized within transpressional shear zones at ca. 290 Ma.
689 These shear zones show "top to the north" (i.e., reverse) kinematics, which is the opposite of
690 well-known transpressional shear zones from the rest of the Axial Zone.

691 By integrating these structural observations at a larger scale, we show that the Axial Zone forms a
692 symmetrical doubly verging accretionary domain where horizontal shortening is accommodated
693 by i) N-S compression yielding northward and southward extrusion of the thickening upper crust
694 by thrusting and ii) horizontal orogen-parallel extrusion of the partially molten lower crust, which
695 is typical of hot orogens. The gravity instabilities were enhanced within the granulitic crust in
696 several NPM, leading to local transverse extension. The evocation of a Late Variscan NPF as a
697 transfer zone or a lithospheric-scale dextral shear zone is not a necessary condition to explain the
698 differences between these neighboring Variscan massifs. As illustrated here, strain was
699 partitioned at the scale of the whole southern part of the Variscides. At the scale of the Variscan
700 belt, we propose that the nonrigid (i.e., weak) Pangea plate was affected by intense continental
701 mass reorganization at the Carboniferous-Permian boundary, leading to the formation of several
702 transpressional restraining bends, like the Cantabrian and Axial Zone bend, coevally with
703 oroclinal bending and continental block rotations. The differences in finite strain patterns
704 between the Variscan belt and other bent hot orogens result from contrasted initial and boundary

conditions, such as the geometry of the strong vs weak lithosphere domains, the orientation of the early belts with respect to the late-compressive stress, and the location of the free edges. In the Variscan belt, the eastward escape of the crust from the Cantabrian-Axial Zone restraining bend could be explained by the presence of a free edge to the east, corresponding to the Paleotethys realm, in a context of Pangea self-subduction.

Acknowledgment

This work was supported by the BRGM through the Référentiel Géologique de la France program (RGF). The redaction of this paper has been permitted thanks to the funding from the Labex Volaire (ANR-10-LABX-100-01) based at Orléans University and BRGM. The newly acquired structural data will be available on the RGF website (www.rgf.brgm.fr). We acknowledge J. R. Martínez Catalán, C. Teyssier, G. Vignaroli and an anonymous reviewer for helping to improve the manuscript, as well as F. Rossetti for the editorial handling.

References

Aguilar, C., Liesa, M., Castiñeiras, P., Navidad, M., 2014. Late Variscan metamorphic and magmatic evolution in the eastern Pyrenees revealed by U–Pb age zircon dating. Journal of the Geological Society 171, 181–192. https://doi.org/10.1144/jgs2012-086

Aguilar, C., Liesa, M., Štípská, P., Schulmann, K., Muñoz, J.A., Casas, J.M., 2015. P–T–t–d evolution of orogenic middle crust of the Roc de Frausa Massif (Eastern Pyrenees): a result of horizontal crustal flow and Carboniferous doming? Journal of Metamorphic Geology 33, 273–294. https://doi.org/10.1111/jmg.12120

Alonso, J.L., Marcos, A., Suárez, A., 2009. Paleogeographic inversion resulting from large out of sequence breaching thrusts: The León Fault (Cantabrian Zone, NW Iberia). A new picture of the external Variscan Thrust Belt in the Ibero-Armorican Arc. Geologica Acta 7, 451–473. https://doi.org/10.1344/105.000001449

729 Andrieux, P., 1982. Conditions de cristallisation et évolution paragénétique d'une charnockite
730 hercynienne : le complexe granulitique d'Ansignan (Massif de l'Agly, Pyrénées-
731 Orientales). Bulletin de Minéralogie 105, 253–266.
732 https://doi.org/10.3406/bulmi.1982.7613
733 Angì, G., Cirrincione, R., Fazio, E., Fiannacca, P., Ortolano, G., Pezzino, A., 2010. Metamorphic
734 evolution of preserved Hercynian crustal section in the Serre Massif (Calabria–Peloritani
735 Orogen, southern Italy). Lithos 115, 237–262. https://doi.org/10.1016/j.lithos.2009.12.008
736 Arthaud, F., Matte, Ph., 1975. Les decrochements tardi-hercyniens du sud-ouest de l'europe.
737 Geometrie et essai de reconstitution des conditions de la deformation. Tectonophysics 25,
738 139–171. https://doi.org/10.1016/0040-1951(75)90014-1
739 Authemayou, C., Le Gall, B., Caroff, M., & Bussien Grosjean, D. (2019). Wrench-related dome
740 formation and subsequent orogenic syntax bending in a hot orogen (Variscan Ibero-
741 Armorican Arc, the Ouessant Island, France). Tectonics 38, 3563–3585.
742 https://doi.org/10.1029/2018TC005189
743 Autran, A., Fonteilles, M., Guitard, G., 1970. Relations entre les intrusions de granitoides,
744 l'anatexie et le metamorphisme regional considerees principalement du point de vue du
745 role de l'eau; cas de la chaine hercynienne des Pyrenees orientales. Bulletin de La Société
746 Géologique de France S7-XII, 673–731. https://doi.org/10.2113/gssgfbull.S7-XII.4.673
747 Ayora, C., Liesa, M., Delgado, J., 1993. Low-thermal-gradient Hercynian metamorphism in the
748 eastern Pyrenees. Journal of Metamorphic Geology 11, 49–58.
749 https://doi.org/10.1111/j.1525-1314.1993.tb00130.x
750 Bahamonde, J.R., Merino-Tomé, O.A., Heredia, N., 2007. A Pennsylvanian microbial
751 boundstone-dominated carbonate shelf in a distal foreland margin (Picos de Europa
752 Province, NW Spain). Sedimentary Geology 198, 167–193.
753 https://doi.org/10.1016/j.sedgeo.2006.12.004
754 Bajolet, F., Chardon, D., Martinod, J., Gapais, D., Kermarrec, J.-J., 2015. Synconvergence flow
755 inside and at the margin of orogenic plateaus: Lithospheric-scale experimental approach.
756 Journal of Geophysical Research: Solid Earth 120, 2015JB012110.
757 https://doi.org/10.1002/2015JB012110
758 Bajolet, F., Replumaz, A., Lainé, R., 2013. Orocline and syntaxes formation during subduction
759 and collision. Tectonics 32, 1529–1546. https://doi.org/10.1002/tect.20087

760 Ballèvre, M., Catalán, J.R.M., López-Carmona, A., Pitra, P., Abati, J., Fernández, R.D.,
761 Ducassou, C., Arenas, R., Bosse, V., Castiñeiras, P., Fernández-Suárez, J., Barreiro, J.G.,
762 Paquette, J.-L., Peucat, J.-J., Poujol, M., Ruffet, G., Martínez, S.S., 2014. Correlation of
763 the nappe stack in the Ibero-Armorican arc across the Bay of Biscay: a joint French–
764 Spanish project. Geological Society, Special Publications 405, 77–113.
765 https://doi.org/10.1144/SP405.13
766 Barbey, P., Villaros, A., Marignac, C., Montel, J.-M., 2015. Multiphase melting, magma
767 emplacement and P-T-time path in late-collisional context: the Velay example (Massif
768 Central, France). Bulletin de La Société Géologique de France 186, 93–116.
769 https://doi.org/10.2113/gssgfbull.186.2-3.93
770 Beaumont, C., Jamieson, R.A., Nguyen, M.H., Lee, B., 2001. Himalayan tectonics explained by
771 extrusion of a low-viscosity crustal channel coupled to focused surface denudation.
772 Nature 414, 738–742. https://doi.org/10.1038/414738a
773 Blanco-Ferrera, S., Sanz-López, J., García-López, S., Bastida, F., 2017. Tectonothermal
774 evolution of the northeastern Cantabrian zone (Spain). International Journal of Earth
775 Sciences 106, 1539–1555. https://doi.org/10.1007/s00531-016-1365-5
776 Bosboom, R., Dupont-Nivet, G., Huang, W., Yang, W., Guo, Z., 2014. Oligocene clockwise
777 rotations along the eastern Pamir: Tectonic and paleogeographic implications. Tectonics
778 33, 53–66. https://doi.org/10.1002/2013TC003388
779 Brun, J.-P., 2002. Deformation of the continental lithosphere: Insights from brittle-ductile
780 models. Geological Society, Special Publications 200, 355–370.
781 https://doi.org/10.1144/GSL.SP.2001.200.01.20
782 Burg, J.-P., Van Den Driessche, J., Brun, J.-P., 1994. Syn- to post-thickening extension in the
783 Variscan Belt of Western Europe: Modes and structural consequences. Géologie de La
784 France 33–51.
785 Buzzi, L., Gaggero, L., 2008. Petrogenesis of post – orogenic Lower Permian andesites in
786 southern Europe: insights into the collapse of the Variscan range. Geodinamica Acta 21,
787 273–290. https://doi.org/10.3166/ga.21.273-290
788 Cagnard, F., Durrieu, N., Gapais, D., Brun, J.-P., Ehlers, C., 2006. Crustal thickening and lateral
789 flow during compression of hot lithospheres, with particular reference to Precambrian
790 times. Terra Nova 18, 72–78. https://doi.org/10.1111/j.1365-3121.2005.00665.x

Cagnard, F., Gapais, D., Barbey, P., 2007. Collision tectonics involving juvenile crust: The example of the southern Finnish Svecofennides. Precambrian Research 154, 125–141. https://doi.org/10.1016/j.precamres.2006.12.011

Canérot, J., 2016. The Iberian Plate: myth or reality? Boletín Geológico y Minero 127, 563–574.

Carosi, R., Palmeri, R., 2002. Orogen-parallel tectonic transport in the Variscan belt of northeastern Sardinia (Italy): implications for the exhumation of medium-pressure metamorphic rocks. Geological Magazine 139, 497–511. https://doi.org/10.1017/S0016756802006763

Carreras, J., 2001. Zooming on Northern Cap de Creus shear zones. Journal of Structural Geology 23, 1457–1486. https://doi.org/10.1016/S0191-8141(01)00011-6

Carreras, J., Capella, I., 1994. Structures and Tectonics at Different Lithospheric Levels Tectonic levels in the Palaeozoic basement of the Pyrenees: a review and a new interpretation. Journal of Structural Geology 16, 1509–1524. https://doi.org/10.1016/0191-8141(94)90029-9

Carreras, J., Druguet, E., 2014. Framing the tectonic regime of the NE Iberian Variscan segment. Geological Society, Special Publications 405, 249–264. https://doi.org/10.1144/SP405.7

Carreras, J., Julivert, M., Santanach, P., 1980. Hercynian mylonite belts in the eastern Pyrenees: an example of shear zones associated with late folding. Journal of Structural Geology 2, 1/2, 5-9.

Casas, J.M., Fernández, O., Domingo, F., 2007. Carboniferous normal faults in the Eastern Pyrenees: evidences and age constrains of syn-orogenic Variscan extension. Geodinamica Acta 20, 385–392. https://doi.org/10.3166/ga.20.385-392

Casini, L., Cuccuru, S., Maino, M., Oggiano, G., Tiepolo, M., 2012. Emplacement of the Arzachena Pluton (Corsica–Sardinia Batholith) and the geodynamics of incoming Pangaea. Tectonophysics 544–545, 31–49. https://doi.org/10.1016/j.tecto.2012.03.028

Casini, L., Cuccuru, S., Puccini, A., Oggiano, G., Rossi, Ph., 2015. Evolution of the Corsica–Sardinia Batholith and late-orogenic shearing of the Variscides. Tectonophysics 646, 65–78. https://doi.org/10.1016/j.tecto.2015.01.017

Chardon, D., Gapais, D., Cagnard, F., 2009. Flow of ultra-hot orogens: A view from the Precambrian, clues for the Phanerozoic. Tectonophysics 477, 105–118. https://doi.org/10.1016/j.tecto.2009.03.008

Chardon, D., Jayananda, M., Peucat, J.-J., 2011. Lateral constrictional flow of hot orogenic crust: Insights from the Neoarchean of south India, geological and geophysical implications for orogenic plateaux. Geochemistry, Geophysics, Geosystems 12, Q02005. https://doi.org/10.1029/2010GC003398

Choulet, F., Faure, M., Fabbri, O., Monié, P., 2012. Relationships between magmatism and extension along the Autun–La Serre fault system in the Variscan Belt of the eastern French Massif Central. International Journal of Earth Sciences 101, 393–413. https://doi.org/10.1007/s00531-011-0673-z

Clark, M.K., Royden, L.H., 2000. Topographic ooze: Building the eastern margin of Tibet by lower crustal flow. Geology 28, 703–706. https://doi.org/10.1130/0091-7613(2000)28<703:TOBTEM>2.0.CO;2

Cochelin, B., Chardon, D., Denèle, Y., Gumiaux, C., Le Bayon, B., 2017. Vertical strain partitioning in hot Variscan crust: Syn-convergence escape of the Pyrenees in the Iberian-Armorican syntax. Bulletin de la Société géologique de France 188, 39. https://doi.org/10.1051/bsgf/2017206

Cochelin, B., Gumiaux, C., Chardon, D., Denèle, Y., Le Bayon, B., 2018a. Multi-scale strainfield analysis using geostatistics: Investigating the rheological behavior of the hot Variscan crust of the Pyrenees (Axial Zone). Journal of Structural Geology 116, 114–130. https://doi.org/10.1016/j.jsg.2018.07.024

Cochelin, B., Lemirre, B., Denèle, Y., Blanquat, M. de S., Lahfid, A., Duchêne, S., 2018b. Structural inheritance in the Central Pyrenees: the Variscan to Alpine tectonometamorphic evolution of the Axial Zone. Journal of the Geological Society 175, 336–351. https://doi.org/10.1144/jgs2017-066

Conand, C., Mouthereau, F., Ganne, J., Lin, A.T.-S., Lahfid, A., Daudet, M., Mesalles, L., Giletycz, S., Bonzani, M., 2020. Strain Partitioning and Exhumation in Oblique Taiwan Collision: Role of Rift Architecture and Plate Kinematics. Tectonics 39, e2019TC005798. https://doi.org/10.1029/2019TC005798

Corsini, M., Rolland, Y., 2009. Late evolution of the southern European Variscan belt: Exhumation of the lower crust in a context of oblique convergence. Comptes Rendus Geoscience, Mécanique de l'orogénie Varisque : Une Vision Moderne de Le Recherche

Dans Le Domaine de l'orogénieMechanics of Variscan Orogeny: A Modern View on Orogenic Research 341, 214–223. https://doi.org/10.1016/j.crte.2008.12.002

Davy, Ph., Cobbold, P.R., 1991. Experiments on shortening of a 4-layer model of the continental lithosphere. Tectonophysics 188, 1–25. https://doi.org/10.1016/0040-1951(91)90311-F

Debon, F., Enrique, P., Autran, A., 1996. Magmatisme hercynien. Synthèse Géologique et Géophysique Des Pyrénées vol. 1, Orléans (France), BRGM-ITGE, 361–499.

Debon, F., Guitard, G., 1996. Carte de synthese metamorphisme et plutonisme hercyniens. Synthèse Géologique et Géophysique Des Pyrénées vol. 1, Orléans (France), BRGM-ITGE.

Delaperrière, E., Blanquat, M. de S., Brunel, M., Lancelot, J.R., 1994. Geochronologie U-Pb sur zircons et monazites dans le massif du Saint Barthelemy (Pyrenees, France); discussion des ages des evenements varisques et pre-varisques. Bulletin de La Societe Geologique de France 165, 101–112.

Delchini, S., Lahfid, A., Lacroix, B., Baudin, T., Hoepffner, C., Guerrot, C., Lach, P., Saddiqi, O., Ramboz, C., 2018. The Geological Evolution of the Variscan Jebilet Massif, Morocco, Inferred From New Structural and Geochronological Analyses. Tectonics 37, 4470–4493. https://doi.org/10.1029/2018TC005002

Delvolvé, J.-J., Perret, M.-F., 1989. Variation de l'âge des sediments calcaires et "Culm" carbonifère dans la chaine varisque du sud de la France : migration de l'orogenèse varisque. Geodinamica Acta 3, 117–126.

Denèle, Y., Laumonier, B., Paquette, J.-L., Olivier, P., Gleizes, G., Barbey, P., 2014. Timing of granite emplacement, crustal flow and gneiss dome formation in the Variscan segment of the Pyrenees. Geological Society, Special Publications 405, 265–287. https://doi.org/10.1144/SP405.5

Denèle, Y., Olivier, P., Gleizes, G., 2008. Progressive deformation of a zone of magma transfer in a transpressional regime: The Variscan Mérens shear zone (Pyrenees, France). Journal of Structural Geology 30, 1138–1149. https://doi.org/10.1016/j.jsg.2008.05.006

Denèle, Y., Olivier, P., Gleizes, G., Barbey, P., 2009. Decoupling between the middle and upper crust during transpression-related lateral flow: Variscan evolution of the Aston gneiss dome (Pyrenees, France). Tectonophysics 477, 244–261. https://doi.org/10.1016/j.tecto.2009.04.033

Denèle, Y., Olivier, P., Gleizes, G., Barbey, P., 2007. The Hospitalet gneiss dome (Pyrenees) revisited: lateral flow during Variscan transpression in the middle crust. Terra Nova 19, 445–453. https://doi.org/10.1111/j.1365-3121.2007.00770.x

Denèle, Y., Paquette, J.-L., Olivier, P., Barbey, P., 2012. Permian granites in the Pyrenees: the Aya pluton (Basque Country). Terra Nova 24, 105–113. https://doi.org/10.1111/j.1365-3121.2011.01043.x

de Hoÿm de Marien, L., Le Bayon, B., Pitra, P., Van Den Driessche, J., Poujol, M., Cagnard, F., 2019. Two-stage Variscan metamorphism in the Canigou massif: Evidence for crustal thickening in the Pyrenees. Journal of Metamorphic Geology 37, 863–888. https://doi.org/10.1111/jmg.12487

Díez Fernández, R., Martínez Catalán, J.R., Barreiro, J.G., Arenas, R., 2012. Extensional Flow during Gravitational Collapse: A Tool for Setting Plate Convergence (Padrón Migmatitic Dome, Variscan Belt, NW Iberia). The Journal of Geology 120, 83–103. https://doi.org/10.1086/662735

Díez Fernández, R., Pereira, M.F., 2017. Strike-slip shear zones of the Iberian Massif: Are they coeval? Lithosphere 9, 726–744. https://doi.org/10.1130/L648.1

Druguet, E., 2001. Development of high thermal gradients by coeval transpression and magmatism during the Variscan orogeny: insights from the Cap de Creus (Eastern Pyrenees). Tectonophysics 332, 275-293.

Druguet, E., Castro, A., Chichorro, M., Pereira, M.F., Fernández, C., 2014. Zircon geochronology of intrusive rocks from Cap de Creus, Eastern Pyrenees. Geological Magazine 151, 1095–1114. https://doi.org/10.1017/S0016756814000041

Ducassou, C., Mercuzot, M., Bourquin, S., Rossignol, C., Pellenard, P., Beccaletto, L., Poujol, M., Hallot, E., Pierson-Wickmann, A.C., Hue, C., Ravier, E., 2019. Sedimentology and U-Pb dating of Carboniferous to Permian continental series of the northern Massif Central (France): Local palaeogeographic evolution and larger scale correlations. Palaeogeography, Palaeoclimatology, Palaeoecology 533, 109228. https://doi.org/10.1016/j.palaeo.2019.06.001

Echtler, H., Malavieille, J., 1990. Extensional tectonics, basement uplift and Stephano-Permian collapse basin in a late Variscan metamorphic core complex (Montagne Noire, Southern Massif Central). Tectonophysics 177, 125–138.

914 Edel, J.-B., Casini, L., Oggiano, G., Rossi, P., Schulmann, K., 2014. Early Permian 90°
915 clockwise rotation of the Maures–Estérel–Corsica–Sardinia block confirmed by new
916 palaeomagnetic data and followed by a Triassic 60° clockwise rotation. Geological
917 Society, Special Publications 405, 333–361. https://doi.org/10.1144/SP405.10
918 Edel, J.B., Schulmann, K., Lexa, O., Lardeaux, J.M., 2018. Late Palaeozoic palaeomagnetic and
919 tectonic constraints for amalgamation of Pangea supercontinent in the European Variscan
920 belt. Earth-Science Reviews 177, 589–612.
921 https://doi.org/10.1016/j.earscirev.2017.12.007
922 Escuder Viruete, J., Hernáiz Huerta, P.P., Valverde-Vaquero, P., Rodríguez Fernández, R.,
923 Dunning, G., 1998. Variscan syncollisional extension in the Iberian Massif: structural,
924 metamorphic and geochronological evidence from the Somosierra sector of the Sierra de
925 Guadarrama (Central Iberian Zone, Spain). Tectonophysics 290, 87–109.
926 Esteban, J.J., Aranguren, A., Cuevas, J., Hilario, A., Tubía, J.M., Larionov, A., Sergeev, S., 2015.
927 Is there a time lag between the metamorphism and emplacement of plutons in the Axial
928 Zone of the Pyrenees? Geological Magazine 152, 935–941.
929 https://doi.org/10.1017/S001675681500014X
930 Evans, N.G., 1993. Deformation during the emplacement of the Maladeta granodiorite, Spanish
931 Pyrenees. PhD thesis, University of Leeds.
932 Evans, N.G., Gleizes, G., Leblanc, D., Bouchez, J.L., 1998. Syntectonic emplacement of the
933 Maladeta granite (Pyrenees) deduced from relationships between Hercynian deformation
934 and contact metamorphism. Journal of the Geological Society 155, 209–216.
935 https://doi.org/10.1144/gsjgs.155.1.0209
936 Faure, M., Lardeaux, J.-M., Ledru, P., 2009. A review of the pre-Permian geology of the
937 Variscan French Massif Central. Comptes Rendus Geoscience, 341, 202–213.
938 https://doi.org/10.1016/j.crte.2008.12.001
939 Faure, M., Prost, A.E., Lasne, E., 1990. Déformation ductile extensive d'âge namuro-westphalien
940 dans le plateau d'Aigurande, Massif central français. Bullutin de la Société Géologique de
941 France 8, 189–197.
942 Fossen, H., Cavalcante, G.C.G., 2017. Shear zones - A review. Earth-Science Reviews 171, 434-
943 455. http://dx.doi.org/10.1016/j.earscirev.2017.05.002

Franke, W., 2014. Topography of the Variscan orogen in Europe: failed–not collapsed. International Journal of Earth Sciences 103, 1471–1499. https://doi.org/10.1007/s00531-014-1014-9

Fréville, K., Trap, P., Faure, M., Melleton, J., Li, X.-H., Lin, W., Blein, O., Bruguier, O., Poujol, M., 2018. Structural, metamorphic and geochronological insights on the Variscan evolution of the Alpine basement in the Belledonne Massif (France). Tectonophysics 726, 14–42. https://doi.org/10.1016/j.tecto.2018.01.017

Gapais, D., 1989. Shear structures within deformed granites: Mechanical and thermal indicators. Geology 17, 1144–1147. https://doi.org/10.1130/0091-7613(1989)017<1144:SSWDGM>2.3.CO;2

Gapais, D., Brun, J.-P., Gumiaux, C., Cagnard, F., Ruffet, G., Le Carlier De Veslud, C., 2015. Extensional tectonics in the Hercynian Armorican belt (France). An overview. Bulletin de La Société Géologique de France 186, 117–129. https://doi.org/10.2113/gssgfbull.186.2-3.117

Gapais, D., Cagnard, F., Gueydan, F., Barbey, P., Ballèvre, M., 2009. Mountain building and exhumation processes through time: inferences from nature and models. Terra Nova 21, 188–194. https://doi.org/10.1111/j.1365-3121.2009.00873.x

Gapais, D., Pêcher, A., Gilbert, E., Ballèvre, M., 1992. Synconvergence spreading of the higher Himalaya crystalline in Ladakh. Tectonics 11, 1045–1056. https://doi.org/10.1029/92TC00819

Gapais, D., Potrel, A., Machado, N., Hallot, E., 2005. Kinematics of long-lasting Paleoproterozoic transpression within the Thompson Nickel Belt, Manitoba, Canada. Tectonics 24. https://doi.org/10.1029/2004TC001700

García-López, S., Voldman, G.G., Bastida, F., Aller, J., 2018. Tectonothermal analysis of a major unit of the Cantabrian Zone: the Ponga unit (Variscan belt, NW Spain). International Journal of Earth Sciences 107, 2727–2740. https://doi.org/10.1007/s00531-018-1623-9

García-Sansegundo, J., Poblet, J., Alonso, J.L., Clariana, P., 2011. Hinterland-foreland zonation of the Variscan orogen in the Central Pyrenees: comparison with the northern part of the Iberian Variscan Massif. Geological Society, Special Publications 349, 169–184. https://doi.org/10.1144/SP349.9

974 Genna, A., Roig, J.-Y., Debriette, J.-P., Bouchot, V., 1998. Le bassin houiller d'Argentat (Massif
975 central français), conséquence topographique d'un plissement de son substratum varisque.
976 C. R. Acad. Sci. Paris 327, 279–284.
977 Giró, E., Alías López, G., 2007. Evolución metamórfica de las kinzigitas en facies granulita del
978 macizo del Aglí. Geogaceta 41, 95–98.
979 Gleizes, G., Crevon, G., Asrat, A., Barbey, P., 2006. Structure, age and mode of emplacement of
980 the Hercynian Bordères-Louron pluton (Central Pyrenees, France). International Journal
981 of Earth Sciences 95, 1039–1052. https://doi.org/10.1007/s00531-006-0088-4
982 Gleizes, G., Leblanc, D., Bouchez, J.L., 1998. The main phase of the Hercynian orogeny in the
983 Pyrenees is a dextral transpression. Geological Society, Special Publications 135, 267–
984 273. https://doi.org/10.1144/GSL.SP.1998.135.01.17
985 Gleizes, G., Leblanc, D., Olivier, P., Bouchez, J., 2001. Strain partitioning in a pluton during
986 emplacement in transpressional regime: the example of the Néouvielle granite (Pyrenees).
987 International Journal of Earth Sciences 90, 325–340.
988 https://doi.org/10.1007/s005310000144
989 Gretter, N., Ronchi, A., López-Gómez, J., Arche, A., De la Horra, R., Barrenechea, J., Lago, M.,
990 2015. The Late Palaeozoic-Early Mesozoic from the Catalan Pyrenees (Spain): 60 Myr of
991 environmental evolution in the frame of the western peri-Tethyan palaeogeography.
992 Earth-Science Reviews 150, 679–708. https://doi.org/10.1016/j.earscirev.2015.09.001
993 Guerrot, C., 2001. Résultats de datation U-Pb par dissolution sur zircons pour l'échantillon
994 SRYN37-1, Maroc. Rapport technique BRGM No. ANA H4028A.
995 Guitard, G., Vielzeuf, D., Martinez, F., 1996. Métamorphisme hercynien. Synthèse Géologique et
996 Géophysique Des Pyrénées vol. 1, Orléans (France), Edition BRGM - ITGE, 501–584.
997 Gutiérrez-Alonso, G., Fernández-Suárez, J., Weil, A.B., 2004. Orocline triggered lithospheric
998 delamination. Geological Society of America Special Papers 383, 121–130.
999 https://doi.org/10.1130/0-8137-2383-3(2004)383[121:OTLD]2.0.CO;2
1000 Gutiérrez-Alonso, G., Fernández-Suárez, J., Weil, A.B., Brendan Murphy, J., Damian Nance, R.,
1001 Corfú, F., Johnston, S.T., 2008. Self-subduction of the Pangaean global plate. Nature
1002 Geoscience 1, 549–553. https://doi.org/10.1038/ngeo250

Gutiérrez-Alonso, G., Johnston, S.T., Weil, A.B., Pastor-Galán, D., Fernández-Suárez, 2012. Buckling an orogen: The Cantabrian Orocline. GSA Today 22, 4–9. https://doi.org/10.1130/GSATG141A.1

Hart, N.R., Stockli, D.F., Hayman, N.W., 2016. Provenance evolution during progressive rifting and hyperextension using bedrock and detrital zircon U-Pb geochronology, Mauléon Basin, western Pyrenees. Geosphere 12, 1166–1186. https://doi.org/10.1130/GES01273.1

Hernández Enrile, J.L., 1991. Extensional tectonics of the toledo ductile-brittle shear zone, central Iberian Massif. Tectonophysics 191, 311–324. https://doi.org/10.1016/0040-1951(91)90064-Y

Jamieson, R.A., Beaumont, C., 2011. Coeval thrusting and extension during lower crustal ductile flow – implications for exhumation of high-grade metamorphic rocks. Journal of Metamorphic Geology 29, 33–51. https://doi.org/10.1111/j.1525-1314.2010.00908.x

Jammes, S., Manatschal, G., Lavier, L., Masini, E., 2009. Tectonosedimentary evolution related to extreme crustal thinning ahead of a propagating ocean: Example of the western Pyrenees. Tectonics 28, TC4012. https://doi.org/10.1029/2008TC002406

Johnston, S.T., Weil, A.B., Gutiérrez-Alonso, G., 2013. Oroclines: Thick and thin. GSA Bulletin 125, 643–663. https://doi.org/10.1130/B30765.1

Jolivet, L., Romagny, A., Gorini, C., Maillard, A., Thinon, I., Couëffé, R., Ducoux, M., Séranne, M., 2020. Fast dismantling of a mountain belt by mantle flow: Late-orogenic evolution of Pyrenees and Liguro-Provençal rifting. Tectonophysics 776, 228312. https://doi.org/10.1016/j.tecto.2019.228312

Kilzi, M.A., 2014. Etude pétro-géochimique des formations mafiques et ultramafiques associées aux formations granulitiques, métamorphiques et anatectiques des Pyrénées hercyniennes (massif du Castillon et massif de Gavarnie). PhD thesis, Université Paul Sabatier, Toulouse, France.

Kilzi, M.A., Grégoire, M., Bosse, V., Benoît, M., Driouch, Y., de Saint Blanquat, M., Debat, P., 2016. Geochemistry and zircon U–Pb geochronology of the ultramafic and mafic rocks emplaced within the anatectic series of the Variscan Pyrenees: The example of the Gavarnie–Heas dome (France). Comptes Rendus Geoscience 348, 107–115. https://doi.org/10.1016/j.crte.2015.06.014

Kretz, R., 1983. Symbols for rock-forming minerals. American Mineralogist 68, 277–279.

Krýza, O., Závada, P., Lexa, O., 2019. Advanced strain and mass transfer analysis in crustal-scale oroclinal buckling and detachment folding analogue models. Tectonophysics 764, 88–109. https://doi.org/10.1016/j.tecto.2019.05.001

Kunz, B.E., Manzotti, P., von Niederhäusern, B., Engi, M., Darling, J.R., Giuntoli, F., Lanari, P., 2018. Permian high-temperature metamorphism in the Western Alps (NW Italy). International Journal of Earth Sciences 107, 203–229. https://doi.org/10.1007/s00531-017-1485-6

Laurent, O., Couzinié, S., Zeh, A., Vanderhaeghe, O., Moyen, J.-F., Villaros, A., Gardien, V., Chelle-Michou, C., 2017. Protracted, coeval crust and mantle melting during Variscan late-orogenic evolution: U–Pb dating in the eastern French Massif Central. International Journal of Earth Sciences 106, 421–451. https://doi.org/10.1007/s00531-016-1434-9

Le Bayon, B., Cochelin, B., 2020. Anatomy of an extensional shear zone leading to the exhumation of the middle crust within the Canigou dome (Eastern Pyrenees, Axial Zone). Journal of Structural Geology 141, 104200. https://doi.org/10.1016/j.jsg.2020.104200

Leblanc, D., Gleizes, G., Roux, L., Bouchez, J.L., 1996. Variscan dextral transpression in the French Pyrenees: new data from the Pic des Trois-Seigneurs granodiorite and its country rocks. Tectonophysics 261, 331–345. https://doi.org/10.1016/0040-1951(95)00174-3

Ledru, P., Courrioux, G., Dallain, C., Lardeaux, J.M., Montel, J.M., Vanderhaeghe, O., Vitel, G., 2001. The Velay dome (French Massif Central): melt generation and granite emplacement during orogenic evolution. Tectonophysics 342, 207–237. https://doi.org/10.1016/S0040-1951(01)00165-2

Lemirre, B., 2018. Origine et développement de la thermicité dans les Pyrénées varisques. PhD thesis. Université Paul Sabatier, Toulouse, France.

Lemirre, B., Cochelin, B., Duchene, S., de Saint Blanquat, M., Poujol, M., 2019. Origin and duration of late orogenic magmatism in the foreland of the Variscan belt (Lesponne — Chiroulet — Neouvielle area, French Pyrenees). Lithos 336–337, 183–201. https://doi.org/10.1016/j.lithos.2019.03.037

Lloret, J., Ronchi, A., López-Gómez, J., Gretter, N., De la Horra, R., Barrenechea, J.F., Arche, A., 2018. Syn-tectonic sedimentary evolution of the continental late Palaeozoic-early Mesozoic Erill Castell-Estac Basin and its significance in the development of the central

Pyrenees Basin. Sedimentary Geology 374, 134–157. https://doi.org/10.1016/j.sedgeo.2018.07.014

Lopez-Sanchez, M.A., García-Sansegundo, J., Martínez, F.J., 2018. The significance of early Permian and early Carboniferous U–Pb zircon ages in the Bossòst and Lys-Caillaouas granitoids (Pyrenean Axial Zone). Geological Journal 54, 1-16. https://doi.org/10.1002/gj.3283

Lotout, C., Poujol, M., Pitra, P., Anczkiewicz, R., Van Den Driessche, J., 2020. From Burial to Exhumation: Emplacement and Metamorphism of Mafic Eclogitic Terranes Constrained Through Multimethod Petrochronology, Case Study from the Lévézou Massif (French Massif Central, Variscan Belt). Journal of Petrology 61. https://doi.org/10.1093/petrology/egaa046

Martínez Catalán, J.R., 2011. Are the oroclines of the Variscan belt related to late Variscan strike-slip tectonics? Terra Nova 23, 241–247. https://doi.org/10.1111/j.1365-3121.2011.01005.x

Martínez Catalán, J.R., Arenas, R., García, F.D., Cuadra, P.G., Gómez-Barreiro, J., Abati, J., Castiñeiras, P., Fernández-Suárez, J., Martínez, S.S., Andonaegui, P., Clavijo, E.G., Montes, A.D., Pascual, F.J.R., Aguado, B.V., 2007. Space and time in the tectonic evolution of the northwestern Iberian Massif: Implications for the Variscan belt. In: 4-D framework of continental crust (R.D. Hatcher Jr., M.P. Carlson, J.H. McBride and J.R. Martínez Catalán, Eds.). Geological Society of America Memoirs 200, 403–423. https://doi.org/10.1130/2007.1200(21)

Martínez Catalán, J.R., Pascual, F.J.R., Montes, A.D., Fernández, R.D., Barreiro, J.G., Silva, Í.D.D., Clavijo, E.G., Ayarza, P., Alcock, J.E. (2014). The late Variscan HT/LP metamorphic event in NW and Central Iberia: relationships to crustal thickening, extension, orocline development and crustal evolution. Geological Society, Special Publications 405, 225–247. https://doi.org/10.1144/SP405.1

Matte, P., 1986. Tectonics and plate tectonics model for the Variscan belt of Europe. Tectonophysics 126, 329-374.

Matte, P., 1991. Accretionary history and crustal evolution of the Variscan belt in Western Europe. Tectonophysics 196, 309–337. https://doi.org/10.1016/0040-1951(91)90328-P

Matte, P., 2001. The Variscan collage and orogeny (480–290 Ma) and the tectonic definition of the Armorica microplate: a review. Terra Nova 13, 122–128. https://doi.org/10.1046/j.1365-3121.2001.00327.x

Matte, P., 2002. Les plis hercyniens kilométriques couchés vers l'ouest-sud-ouest dans la région du pic du Midi d'Ossau–col du Somport (zone axiale des Pyrénées occidentales). Comptes Rendus Geoscience 334, 773–779.

Maurel, O., Respaut, J.-P., Monié, P., Arnaud, N., Brunel, M., 2004. U-Pb emplacement and 40Ar/39Ar cooling ages of the eastern Mont-Louis granite massif (Eastern Pyrenees, France). Comptes Rendus Geoscience 336, 1091–1098. https://doi.org/10.1016/j.crte.2004.04.005

Mendia, M.S., Ibarguchi, J.I.G., 1991. High-grade metamorphic rocks and peridotites along the Leiza Fault (Western Pyrenees, Spain). Geologische Rundschau 80, 93–107. https://doi.org/10.1007/BF01828769

Merino-Tomé, O.A., Bahamonde, J.R., Colmenero, J.R., Heredia, N., Villa, E., Farias, P., 2009. Emplacement of the Cuera and Picos de Europa imbricate system at the core of the Iberian-Armorican arc (Cantabrian zone, north Spain): New precisions concerning the timing of arc closure. Geological Society of America Bulletin 121, 729–751. https://doi.org/10.1130/B26366.1

Mezger, J.E., 2009. Transpressional tectonic setting during the main Variscan deformation: evidence from four structural levels in the Bossòst and Aston-Hospitalet mantled gneiss domes, central Axial Zone, Pyrenees. Bulletin de La Societe Geologique de France 180, 199–207. https://doi.org/10.2113/gssgfbull.180.3.199

Mezger, J.E., Gerdes, A., 2016. Early Variscan (Visean) granites in the core of central Pyrenean gneiss domes: implications from laser ablation U-Pb and Th-Pb studies. Gondwana Research 29, 181–198. https://doi.org/10.1016/j.gr.2014.11.010

Mezger, J.E., Passchier, C.W., 2003. Polymetamorphism and ductile deformation of staurolite–cordierite schist of the Bossòst dome: indication for Variscan extension in the Axial Zone of the central Pyrenees. Geological Magazine 140, 595–612. https://doi.org/10.1017/S0016756803008112

Mezger, J.E., Passchier, C.W., Régnier, J.-L., 2004. Metastable staurolite–cordierite assemblage of the Bossòst dome: Late Variscan decompression and polyphase metamorphism in the

Axial Zone of the central Pyrenees. Comptes Rendus Geoscience 336, 827–837. https://doi.org/10.1016/j.crte.2003.12.024

Mezger, J.E., Régnier, J.-L., 2016. Stable staurolite–cordierite assemblages in K-poor metapelitic schists in Aston and Hospitalet gneiss domes of the central Pyrenees (France, Andorra). Journal of Metamorphic Geology 34, 167–190. https://doi.org/10.1111/jmg.12177

Michard, A., Soulaimani, A., Hoepffner, C., Ouanaimi, H., Baidder, L., Rjimati, E.C., Saddiqi, O., 2010. The South-Western Branch of the Variscan Belt: Evidence from Morocco. Tectonophysics 492, 1–24. https://doi.org/10.1016/j.tecto.2010.05.021

Moyen, J.-F., Laurent, O., Chelle-Michou, C., Couzinié, S., Vanderhaeghe, O., Zeh, A., Villaros, A., Gardien, V., 2017. Collision vs. subduction-related magmatism: Two contrasting ways of granite formation and implications for crustal growth. Lithos 277, 154–177. https://doi.org/10.1016/j.lithos.2016.09.018

Nirrengarten, M., Manatschal, G., Tugend, J., Kusznir, N., Sauter, D., 2018. Kinematic Evolution of the Southern North Atlantic: Implications for the Formation of Hyperextended Rift Systems. Tectonics 37, 89–118. https://doi.org/10.1002/2017TC004495

Olivier, P., Gleizes, G., Paquette, J.L., 2004. Gneiss domes and granite emplacement in an obliquely convergent regime: New interpretation of the Variscan Agly Massif (Eastern Pyrenees, France). Geological Society of America Special Papers 380, 229–242. https://doi.org/10.1130/0-8137-2380-9.229

Olivier, P., Gleizes, G., Paquette, J.-L., Muñóz Sáez, C., 2008. Structure and U-Pb dating of the Saint-Arnac pluton and the Ansignan charnockite (Agly Massif): a cross-section from the upper to the middle crust of the Variscan Eastern Pyrenees. Journal of the Geological Society 165, 141–152.

Paquette, J.-L., Gleizes, G., Leblanc, D., Bouchez, J.-L., 1997. Le granite de Bassiès (Pyrénées) : un pluton syntectonique d'âge Westphalien. Géochronologie U-Pb sur zircons. Comptes rendus de l'Académie des sciences S2, 324, 387–392.

Pastor-Galán, D., Martín-Merino, G., Corrochano, D., 2014. Timing and structural evolution in the limb of an orocline: The Pisuerga–Carrión Unit (southern limb of the Cantabrian Orocline, NW Spain). Tectonophysics 622, 110–121. https://doi.org/10.1016/j.tecto.2014.03.004

Pastor-Galán, D., Pueyo, E.L., Diederen, M., García-Lasanta, C., Langereis, C.G., 2018. Late Paleozoic Iberian Orocline(s) and the Missing Shortening in the Core of Pangea. Paleomagnetism From the Iberian Range. Tectonics 37, 3877–3892. https://doi.org/10.1029/2018TC004978

Pereira, M.F., Castro, A., Chichorro, M., Fernández, C., Díaz-Alvarado, J., Martí, J., Rodríguez, C., 2014. Chronological link between deep-seated processes in magma chambers and eruptions: Permo-Carboniferous magmatism in the core of Pangaea (Southern Pyrenees). Gondwana Research 25, 290–308. https://doi.org/10.1016/j.gr.2013.03.009

Pérez-Estaún, A., Bastida, F., Alonso, J.L., Marquínez, J., Aller, J., Alvarez-Marrón, J., Marcos, A., Pulgar, J.A., 1988. A thin-skinned tectonics model for an arcuate fold and thrust belt: The Cantabrian Zone (Variscan Ibero-Armorican Arc). Tectonics 7, 517–537. https://doi.org/10.1029/TC007i003p00517

Petri, B., Mohn, G., Skrzypek, E., Mateeva, T., Galster, F., Manatschal, G., 2017. U–Pb geochronology of the Sondalo gabbroic complex (Central Alps) and its position within the Permian post-Variscan extension. International Journal of Earth Sciences 106, 2873–2893. https://doi.org/10.1007/s00531-017-1465-x

Pin, C., Vielzeuf, D., 1983. Granulites and related rocks in Variscan median Europe: A dualistic interpretation. Tectonophysics 93, 47–74. https://doi.org/10.1016/0040-1951(83)90233-0

Poitrenaud, T., 2018. Le gisement périgranitique à tungstène et or de Salau (Pyrénées, France), histoire polyphasée d'un système minéralisé tardi-varisque. PhD thesis, Université d'Orléans, France.

Poitrenaud, T., Poujol, M., Augier, R., Marcoux, E., 2020. The polyphase evolution of a late Variscan W/Au deposit (Salau, French Pyrenees): insights from REE and U/Pb LA-ICP-MS analyses. Mineralium Deposita 55, 1127–1147. https://doi.org/10.1007/s00126-019-00923-2

Pouget, P., 1984. Géologie de la région de Lesponne (Hautes-Pyrénées) = Geology of Lesponne area, Hautes-Pyrénées. PhD thesis, Univ. Paul Sabatier, Toulouse, France.

Pouget, P., 1987. Le massif granitique de Lesponne (Hautes Pyrénées): Un exemple de massif plutonique hercynien à mise en place diapirique syncinématique. Geologische Rundschau 76, 187–199. https://doi.org/10.1007/BF01820582

Pouget, P., 1989. Évolution géodynamique hercynienne des Pyrénées centrales. Contraintes structurales, métamorphiques, magmatiques et sédimentologiques. Thesis, Univ. Paul Sabatier, Toulouse, France.

Pouget, P.P., Lamouroux, C., Dahmani, A., Debat, P., Driouch, Y., Mercier, A., Soula, J.C., Vezat, R., 1989. Typologie et mode de mise en place des roches magmatiques dans les Pyrénées hercyniennes. Geologische Rundschau 78, 537–554. https://doi.org/10.1007/BF01776190

Roberts, M.P., Pin, C., Clemens, J.D., Paquette, J.-L., 2000. Petrogenesis of Mafic to Felsic Plutonic Rock Associations: the Calc-alkaline Quérigut Complex, French Pyrenees. Journal of Petrology 41, 809–844. https://doi.org/10.1093/petrology/41.6.809

Rolin, P., Colchen, M., 2001. Les cisaillements hercyniens de la Vendée au Limousin. Géologie de La France 1–2, 87–116.

Rolland, Y., Corsini, M., Demoux, A., 2009. Metamorphic and structural evolution of the Maures-Tanneron massif (SE Variscan chain): evidence of doming along a transpressional margin. Bulletin de La Société Géologique de France 180, 217–230. https://doi.org/10.2113/gssgfbull.180.3.217

Rolland, Y., Mahéo, G., Guillot, S., Pecher, A., 2001. Tectono-metamorphic evolution of the Karakorum Metamorphic complex (Dassu–Askole area, NE Pakistan): exhumation of mid-crustal HT–MP gneisses in a convergent context. Journal of Metamorphic Geology 19, 717–737. https://doi.org/10.1046/j.0263-4929.2001.00342.x

Rutte, D., Ratschbacher, L., Khan, J., Stübner, K., Hacker, B.R., Stearns, M.A., Enkelmann, E., Jonckheere, R., Pfänder, J.A., Sperner, B., Tichomirowa, M., 2017. Building the Pamir-Tibet Plateau—Crustal stacking, Extensional Collapse, and Lateral Extrusion in the Central Pamir: 2. Timing and Rates. Tectonics 2016TC004294. https://doi.org/10.1002/2016TC004294

de Saint Blanquat, M., Lardeaux, J.M., Brunel, M., 1990. Petrological arguments for high-temperature extensional deformation in the Pyrenean Variscan crust (Saint Barthélémy Massif, Ariège, France). Tectonophysics 233 177, 245–262. https://doi.org/10.1016/0040-1951(90)90284-F

de Saint Blanquat, M. de, 1993. The ductile normal fault of the Saint Barthélémy Massif Variscan evolution of the north-pyrenean catazonal massifs considered from the viewpoint of their

thermal history. Geodinamica Acta 6, 59–77. https://doi.org/10.1080/09853111.1993.11105239

de Sitter, L.U., Zwart, H.J., 1960. Tectonic development in supra and infra-structures of a mountain chain. Proceedings of the 21st International Geological Congress of Cophenhagen 18, 248–256.

Saspiturry, N., Cochelin, B., Razin, P., Leleu, S., Lemirre, B., Bouscary, C., Issautier, B., Serrano, O., Lasseur, E., Baudin, T., Allanic, C., 2019. Tectono-sedimentary evolution of a rift system controlled by Permian post-orogenic extension and metamorphic core complex formation (Bidarray Basin and Ursuya dome, Western Pyrenees). Tectonophysics 768, 228180. https://doi.org/10.1016/j.tecto.2019.228180

Schnapperelle, S., Mezger, J.E., Stipp, M., Hofmann, M., Gärtner, A., Linnemann, U., 2020. Polyphase magmatic pulses along the Northern Gondwana margin: U-Pb zircon geochronology from gneiss domes of the Pyrenees. Gondwana Research 81, 291–311. https://doi.org/10.1016/j.gr.2019.11.013

Siron, G., Goncalves, P., Marquer, D., Pierre, T., Paquette, J.-L., Vanardois, J., 2020. Contribution of magmatism, partial melting buffering and localized crustal thinning on the late Variscan thermal structure of the Agly massif (French Pyrenees). Journal of Metamorphic Geology 38, 799–829. https://doi.org/10.1111/jmg.12549

Stampfli, G.M., Hochard, C., Vérard, C., Wilhem, C., vonRaumer, J., 2013. The formation of Pangea. Tectonophysics 593, 1–19. https://doi.org/10.1016/j.tecto.2013.02.037

Stephenson, B.J., Searle, M.P., Waters, D.J., Rex, D.C., 2001. Structure of the Main Central Thrust zone and extrusion of the High Himalayan deep crustal wedge, Kishtwar–Zanskar Himalaya. Journal of the Geological Society 158, 637–652. https://doi.org/10.1144/jgs.158.4.637

Stipp, M., Stünitz, H., Heilbronner, R. & Schmid, S.M. 2002. The eastern Tonale fault zone: a 'natural laboratory' for crystal plastic deformation of quartz over a temperature range from 250 to 700°C. Journal of Structural Geology 24, 1861–1884, https://doi.org/10.1016/S0191-8141(02)00035-4

Tapponnier, P., Peltzer, G., Dain, A.Y.L., Armijo, R., Cobbold, P., 1982. Propagating extrusion tectonics in Asia: New insights from simple experiments with plasticine. Geology 10, 611–616. https://doi.org/10.1130/0091-7613(1982)10<611:PETIAN>2.0.CO;2

Taylor, M., Yin, A., 2009. Active structures of the Himalayan-Tibetan orogen and their relationships to earthquake distribution, contemporary strain field, and Cenozoic volcanism Active structures on the Tibetan plateau and surrounding regions. Geosphere 5, 199–214. https://doi.org/10.1130/GES00217.1

Ternet, Y., Barrère, P., Canérot, J., Majeste-Menjoulas, C., 2004. Carte géol. France (1/50 000), feuille Laruns-Somport (1069), BRGM, Orléans.

Ternet, Y., Barrère, P., Dallas, S., Debon, F., Debroas, E.J., François, J.-M., Pouget, P., 1996. Carte géol. France (1/50 000), feuille Campan (1071), BRGM, Orléans.

Teyssier, C., Whitney, D.L., 2002. Gneiss domes and orogeny. Geology 30, 1139–1142. https://doi.org/10.1130/0091-7613(2002)030<1139:GDAO>2.0.CO;2

Tikoff, B., Russo, R., Teyssier, C., Tommasi, A., 2004. Mantle-driven deformation of orogenic zones and clutch tectonics. Geological Society, Special Publications 227, 41–64.

Torvela, T., Kurhila, M., 2020. How does orogenic crust deform? Evidence of crustal-scale competent behaviour within the partially molten middle crust during orogenic compression. Precambrian Research 342, 105670. https://doi.org/10.1016/j.precamres.2020.105670

Tournaire Guille, B., 2017. Relation entre magmatisme et métamorphisme Haute-Température Basse-Pression. Réexamen du massif de l'Agly (Pyrénées Orientales). PhD theis, Univ. Paris 6, Paris, France.

Tournaire Guille, B., Olivier, Ph., Paquette, J.-L., Bosse, V., Guillaume, D., 2019. Evolution of the middle crust of the Pyrenees during the Paleozoic: new data on the plutonic rocks from the North Pyrenean Agly Massif. International Journal of Earth Sciences 108, 245–265. https://doi.org/10.1007/s00531-018-1652-4

Triboulet, C., Guitard, G., Katona, I., Navidad, M., 2005. Évolution pression–température des amphibolites de la zone axiale au cours du métamorphisme hercynien des Pyrénées orientales. Comptes Rendus Geoscience 337, 1244–1249. https://doi.org/10.1016/j.crte.2005.06.011

Tugend, J., Manatschal, G., Kusznir, N.J., Masini, E., Mohn, G., Thinon, I., 2014. Formation and deformation of hyperextended rift systems: Insights from rift domain mapping in the Bay of Biscay-Pyrenees. Tectonics 33, 2014TC003529. https://doi.org/10.1002/2014TC003529

Vacherat, A., Mouthereau, F., Pik, R., Huyghe, D., Paquette, J.-L., Christophoul, F., Loget, N., Tibari, B., 2017. Rift-to-collision sediment routing in the Pyrenees: a synthesis from sedimentological, geochronological and kinematic constraints. Earth Science Reviews 172, 43–74. http://dx.doi.org/10.1016/j.earscirev.2017.07.004

Van den Eeckhout, B., Zwart, H.J., 1988. Hercynian crustal-scale extensional shear zone in the Pyrenees. Geology 16, 135–138. https://doi.org/10.1130/0091-7613(1988)016<0135:HCSESZ>2.3.CO;2

Vanardois, J., Trap, P., Goncalves, P., Marquer, D., Gremmel, J., Siron, G., Baudin, T., 2020. Kinematics, deformation partitioning and late Variscan magmatism in the Agly massif, Eastern Pyrenees, France. Bulletin de la Société géologique de France 191. https://doi.org/10.1051/bsgf/2020009

Vanderhaeghe, O., Oscar, L., Gardien, V., Moyen, J.-F., Gébelin, A., Chelle-Michou, C., Couzinié, S., Villaros, A., Bellanger, M., 2020. Flow of partially molten crust controlling construction, growth and collapse of the Variscan orogenic belt: 1 the geologic record of the French Massif Central. Bulletin de la Société géologique de France 191, https://doi.org/10.1051/bsgf/2020013

Vanderhaeghe, O., Teyssier, C., 2001. Partial melting and flow of orogens. Tectonophysics 342, 451–472. https://doi.org/10.1016/S0040-1951(01)00175-5

Van Lichtervelde, M., Grand'Homme, A., Saint-Blanquat, M. de, Olivier, P., Gerdes, A., Paquette, J.-L., Melgarejo, J.C., Druguet, E., Alfonso, P., 2017. U-Pb geochronology on zircon and columbite-group minerals of the Cap de Creus pegmatites, NE Spain. Mineralogy and Petrology 111, 1–21. https://doi.org/10.1007/s00710-016-0455-1

Vielzeuf, D., 1984. Relations de phases dans le faciès granulite et implications géodynamiques: l'exemple des granulites des Pyrénées. PhD thesis, Univ. Clermont Ferrand, France.

Vilà, M., Pin, C., Liesa, M., Enrique, P., 2007. LP-HT metamorphism in a late orogenic transpressional setting, Albera Massif, NE Iberia: implications for the geodynamic evolution of the Variscan Pyrenees. Journal of Metamorphic Geology 25, 321–347. https://doi.org/10.1111/j.1525-1314.2007.00698.x

von Raumer, J.F., Bussy, F., Schaltegger, U., Schulz, B., Stampfli, G.M., 2013. Pre-Mesozoic Alpine basements—Their place in the European Paleozoic framework. GSA Bulletin 125, 89–108. https://doi.org/10.1130/B30654.1

Weil, A., Gutiérrez-alonso, G., Conan, J., 2010. New time constraints on lithospheric-scale oroclinal bending of the Ibero-Armorican Arc: a palaeomagnetic study of earliest Permian rocks from Iberia. Journal of the Geological Society 167, 127–143. https://doi.org/10.1144/0016-76492009-002

Weil, A.B., 2006. Kinematics of orocline tightening in the core of an arc: Paleomagnetic analysis of the Ponga Unit, Cantabrian Arc, northern Spain. Tectonics 25. https://doi.org/10.1029/2005TC001861

Weil, A.B., Gutiérrez-Alonso, G., Johnston, S.T., Pastor-Galán, D., 2013. Kinematic constraints on buckling a lithospheric-scale orocline along the northern margin of Gondwana: A geologic synthesis. Tectonophysics 582, 25–49. https://doi.org/10.1016/j.tecto.2012.10.006

White, A.P., Hodges, K.V., Martin, M.W., Andresen, A., 2002. Geologic constraints on middle-crustal behavior during broadly synorogenic extension in the central East Greenland Caledonides. International Journal of Earth Sciences 91, 187–208. https://doi.org/10.1007/s005310100227

Whitney, D.L., Teyssier, C., Vanderhaeghe, O., 2004. Gneiss domes and crustal flow. Geological Society of America Special Papers 380, 15–33. https://doi.org/10.1130/0-8137-2380-9.15

Worthington, J.R., Ratschbacher, L., Stübner, K., Khan, J., Malz, N., Schneider, S., Kapp, P., Chapman, J.B., Goddard, A.S., Brooks, H.L., Lamadrid, H.M., Steele-MacInnis, M., Rutte, D., Jonckheere, R., Pfänder, J., Hacker, B.R., Oimahmadov, I., Gadoev, M., 2020. The Alichur Dome, South Pamir, Western India–Asia Collisional Zone: Detailing the Neogene Shakhdara–Alichur Syn-collisional Gneiss-Dome Complex and Connection to Lithospheric Processes. Tectonics 39, e2019TC005735. https://doi.org/10.1029/2019TC005735

Yin, A., 2004. Gneiss domes and gneiss dome systems. Geological Society of America Special Papers 380, 1–14.

Zhang, Z., Sun, J., 2020. Cenozoic tectonic rotations in different parts of the NE Pamir: implications for the evolution of the arcuate orogen. International Journal of Earth Sciences 109, 1921–1939. https://doi.org/10.1007/s00531-020-01880-2

Zwart, H.J., 1979. The geology of the Central Pyrenees. Leidse Geol. Mededelingen 50, 1–74.

Figure captions:

Figure 1: Structural sketch of the Variscan belt at late Carboniferous times. Source maps from geodynamic reconstitution are from Franke (2014) for the northern realm of the Variscan belt and Stampfli et al., (2013) for the southern realm (Alleghanian belt, Alpine Mediterranean domain, and Paleotethys) with modifications for Corsica, Sardinia, and Maures-Tanneron relative positions by considering recent paleomagnetic syntheses by Edel et al., (2014, 2018). Directions of stretching are represented only for the 310-290 Ma period, and were synthesized from (1) Michard et al., (2010); (2) review from Martínez Catalán et al., (2014); (3) Cochelin et al., (2017); (4) Corsini and Rolland, (2009); (5) Carosi and Palmeri, (2002); (6) Casini et al., 2012; (7) Choulet et al., (2012); (8) Ledru et al., (2001); (9) Echtler and Malavieille (1990); (10) Faure et al., (1990); (11) Faure et al., (2009); (12) Genna et al., (1998); Rolin and Colchen (2001); (13) Review from Gapais et al., (2015); (14) Saspiturry et al., (2019); (15) Carreras and Debat (1996); (16) de Saint Blanquat (1993); (17) Díez Fernández et al., (2012); (18) Escuder Viruete et al., (1998); (19) Hernández Enrile (1991). Abbreviations: CZ Cantabrian Zone, CIZ: Central Iberian Zone, FMC: French Massif Central, AM: Armorican Massif, BM: Bohemian Massif, MN: Montagne Noire; MT: Maures-Tanneron; CS: Corsica-Sardinia. In the Pyrenees, only the direction of stretching associated with thrusting is shown.

Figure 2: a) Geological map of the Variscan domains of the Pyrenees, modified from Cochelin et al., (2017); (b) Available U-Pb ages for metamorphic rocks and granitoids; (c) P-T diagram showing the P-T paths from the gneiss domes of the Axial Zone, estimations of peak metamorphism and the range of pressure for emplacement of upper crustal plutons. Aston: Mezger and Régnier, (2016); Canigou: de Hoÿme de Marien et al., (2019); Bossost: Mezger et

al., (2004); Roc de France: Aguilar et al., (2015); Albères: Vilà et al., (2007). Range of pressure for pluton emplacement after Autran et al., (1970); Debon et al., (1996); Evans et al., (1998); Poitrenaud, (2018); Synthetic P-T diagrams representing estimations of the metamorphic peak in the Axial Zone (d) and the North Pyrenean Massifs (e). Estimates are from Pouget (1989) ; Ayora et al., (1993); Guitard et al., (1996); Vilà et al., (2007); Mezger and Régnier, (2016) ; Mezger et al., (2004); Triboulet et al., (2005); Lemirre et al., (2019) in the Axial Zone and from Andrieux, (1982); Vielzeuf, (1984); Mendia and Gil Ibarguchi, (1991); de Saint Blanquat et al., (1990); Giró and Alías López, (2007); Tournaire Guille, (2017) ; Siron et al., (2020) for the North Pyrenean Massifs.

Figure 3: Structural map of the Variscan domains from the Pyrenees, modified from Cochelin et al., (2017).

Figure 4: a) Simplified geological map of the studied area, modified from Pouget (1984) and Ternet et al., (1996) with the integration of new field surveys. Cross-sections presented in Figure 6 are localized. A detailed high-resolution geological map is reported in Supporting Information; b) Structural map of the studied area. Foliation trajectories are inferred from Pouget (1984), Ternet et al., (1996), and our measurements; A.R.: Aigue-Rouye sub-dome.

Figure 5: Stereogram of poles to foliation or schistosity (i.e., Si and Ss) in the lower, transitional and upper domains (lower hemisphere; contours=1%). The associated lineations Li or Ls and kinematics are also reported.

Figure 6: Transverse and longitudinal cross-sections across the Chiroulet and Lesponne gneiss domes.

Figure 7: Photographs of gneiss, micaschists, and marbles from the Chiroulet and Lesponne gneiss domes. a) Meter scale sill of porphyritic leucogranite from the Lesponne dome showing a magmatic foliation Si; b) Well-defined shallowly dipping magmatic foliation Si in diorite from the Lesponne dome; c) Mineral lineation (Li) defined by the alignment of biotite, sillimanite, and feldspars within diatexites from the Chiroulet dome. d) Mineral-stretching lineation within amphibolite boudins in migmatites from the Chiroulet dome; e) Domino-like boudinage in calc-silicate gneiss at the top of the migmatites from the Chiroulet dome; f) Interference pattern showing passive reorientation of Li stretching lineation in the hinge of late folds, called Fs (location: Pic du Midi); g) Typical crenulation of the Si foliation by Ss cleavage in the flank of regional folds (location: Pic du Midi); h) stretching striae-lineation Ls associated with Ss foliation within Devonian marbles.

Figure 8: Field photographs of the transitional domain in the southern flank of the Chiroulet dome: a) Panorama of the southern transition between the lower and the transitional domains of the Chiroulet dome, located at the top of migmatites. The difference of deformation patterns is well illustrated, with a poorly disturbed shallowly dipping foliation (Si) in migmatites or Silurian paragneisses and the same fabric in Devonian series that is intensively folded and sheared by reverse shear zones; b) Style of deformation within Lower Devonian marbles and marble/sandstone alternations (location: north-western side of the Lac Bleu), with zooms c) and d) on folded boudins in these layers; e) sub-vertical mylonitic foliation within marble layers and asymmetrical boudinage showing south side up kinematics.

Figure 9: Field photographs from the marbles and schists of the upper domain. a) & a') High-strain fabric in Lower Devonian marbles showing non-coaxial "top to the north" shearing at all scale (location: Lac Bleu, see also Fig. 8); b) Non-coaxial "top to the north" shearing within low-

grade middle Devonian schists in the southern flank of the Lesponne dome; c) Low-grade shear band affecting the diatexites from the Chiroulet dome. Steep C' shears show dextral kinematics; d) & d') Post-Variscan reverse faulting showing reactivation of earlier metamorphic fabric (e.g. Si foliation) and affecting a Permian andesitic dyke (location: north of the Tourmalet pass).

Figure 10: Microphotographs from the various rock types of the Chiroulet and Lesponne area. The cross-section (a) (i.e., cross-section 2 in Figure 6) represents their localization at various structural levels. b) Si foliation in paragneisses, defined by oriented feldspars, quartz, and phyllosilicates. Quartz grains show evidence of deformation bands as well as dynamic recrystallization by grain boundary migration; c) Si foliation and C/S structures in sillimanite-bearing micaschists from the lower domain. Si and C' planes are defined by the alignment of biotite, sillimanite, and quartz layers. Evidence of biotite and sillimanite pinning effect in quartz grain boundaries underline dynamic recrystallization by grain boundary migration; d) Calc-silicate gneiss at the top of the lower domain. Garnet-rich layers are boudinaged and inter-boudins are filled by quartz and calcite-epidote veins. Same sample than shown in Fig. 7e; d') Zoom on the quartz-vein, where quartz grains are recrystallized by grain boundary migration; e) Quartz-rich paragneiss with a core and mantle texture, the core corresponds to garnet and ribbon quart grains (Qtz1) and the mantle to a fine-grained matrix of dynamically recrystallizes quartz (Qtz2) and muscovite; e') Same quartz-rich paragneiss showing Si/Ss relationships. Note that prismatic sillimanites are truncated when reworked by Ss; f) Andalusite-bearing schist where Ss schistosity reworked the Si foliation. Andalusites are partially retrogressed into a fine white mica and chlorite assemblage; f') Zoom on the same rocks showing inclusions of an early fabric within andalusite porphyroclast; f'') Zoom on the same rocks showing dynamically recrystallized quartz grains by sub-grain rotation in the matrix; g and g') Chlorite-muscovite bearing Carboniferous

sandstones showing a dissolution pattern. Quartz grains showing recrystallization by bulging in the matrix and undoluse extinction in porphyroclasts. The cleavage is steeply dipping to the north. Mineral abbreviations are from Kretz, (1983).

Figure 11: Block-diagrams and synthetic P-T diagrams illustrating the three-stage evolution of the Chiroulet and Lesponne area. a) The initiation of the thermal anomaly in the lower crust, leading to the partial melting of the crust. It took place after an earlier stage of deformation D1 that is responsible for the formation of regional NW-SE trending folds. The base of Upper Paleozoic limestones is reached by the thermal anomaly in the regional synclines, allowing significant weakening of the upper crust; b) Between 310 and 300 Ma, the mid-lower crust is partially molten and flows longitudinally under N-S shortening-dominated transpression. Migmatites are partially exhumed from ca. 4.2 kbar to 2.9 kbar, forming gneiss domes due to gravity instabilities and strain partitioning. This is marked by the activation of a decollement level in the thick Devonian marbles. Calc-alkaline plutons intrude the upper crust at this period while smaller dioritic sheets are stocked at the rheological boundary between infrastructure and superstructure; c) The cooling of the crust during N-S convergence led to the final crystallization of magma at 290 Ma, after the emplacement of the leucogranite sheets in gneiss domes. Regional cooling induced strain localization into steep transpressional shear zones and led to amplification of the domal shapes by folding. Abbreviation: WS: Wet Solidus.

Figure 12: Illustration of how strain was partitioned within the Variscan belt in map view (b) and as block-diagrams (a), (c), (d): a) Conceptual model of an opposite direction of extrusion of the crust under convergence and its relationship with local transverse extension in a few North Pyrenean Massif.; b) Localisation of the Pyrenees and the highly shortened domains within the Variscan belt at the Carboniferous-Permian boundary. The Cantabrian Zone and the Pyrenean

Axial Zone form a ca. 100 km wide and 800 km long continuous shortened belt. c) Conceptual model of lateral escape having taken place in the Armorican massif, after Gumiaux et al., (2004) and Gapais et al., (2015); d) Conceptual model of transverse extension in the Eastern Massif Central, after Vanderhaeghe et al., (2020). Further explanation in the text.

Figure 13: Comparison of strain patterns in a context of bending orogenic belts: a) The Variscan belt during the formation of the Cantabrian orocline and late-orogenic plate reorganization, at 305-295 Ma. The thermal state of the lithosphere is considered following the evidence of ductile deformations and metamorphism that took place at 305-295 Ma; b) Main tectonic features of the western edge of the Himalayan-Tibet system. The collision led to westward extrusion of the orogenic plateau during the formation of the Pamir syntax. Modified from Rolland et al., (2001); Vanderhaghe & Teyssier (2001); Rutte et al., (2017) & Worthington et al., (2020). Further details in the text. Abbreviations: CP: Central Pamir; SP: South Pamir, K: Karakorum; MCT: Main Central Thrust; MBT: Main Boundary Thrust; STD: South Tibetan Detachment.

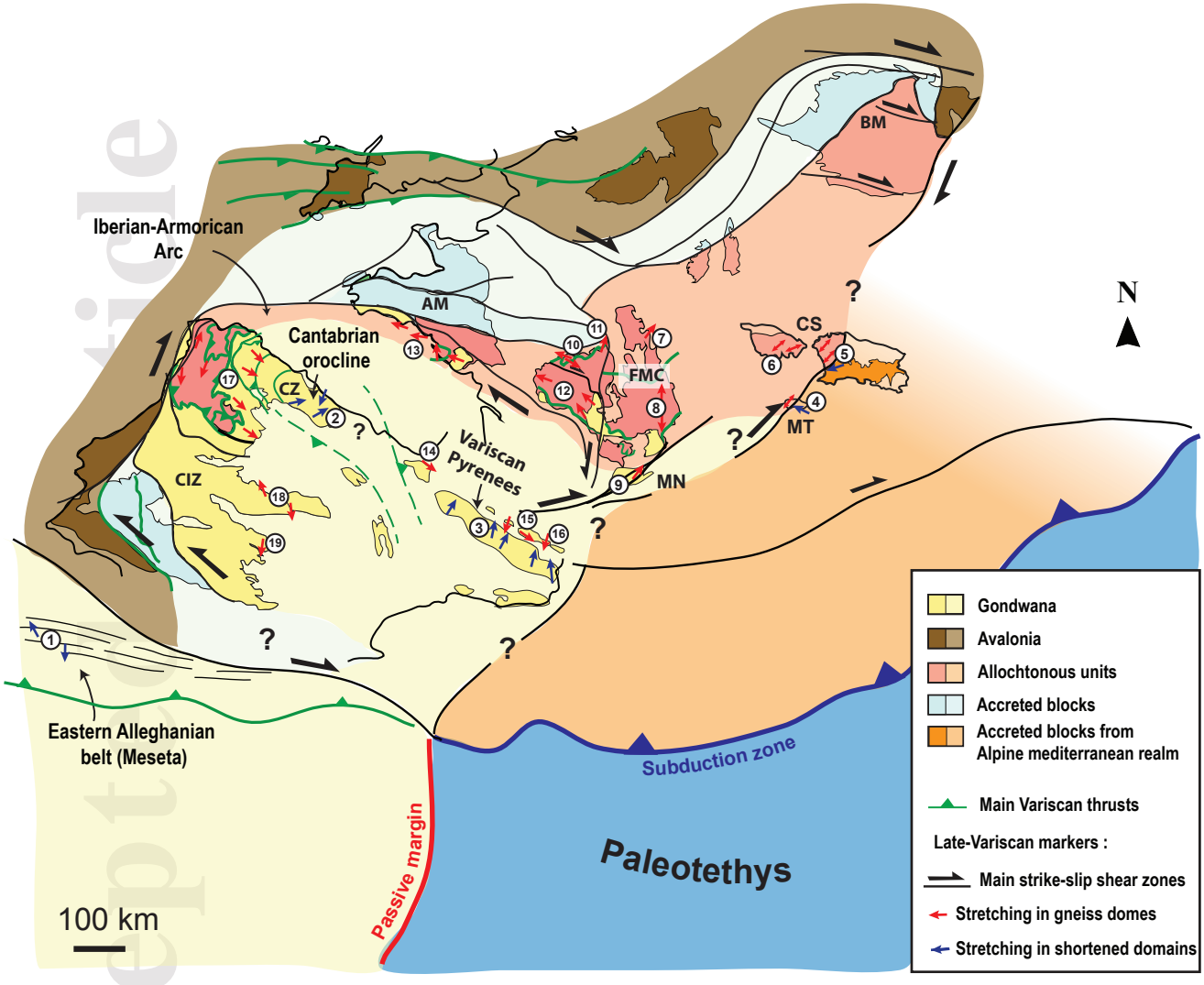

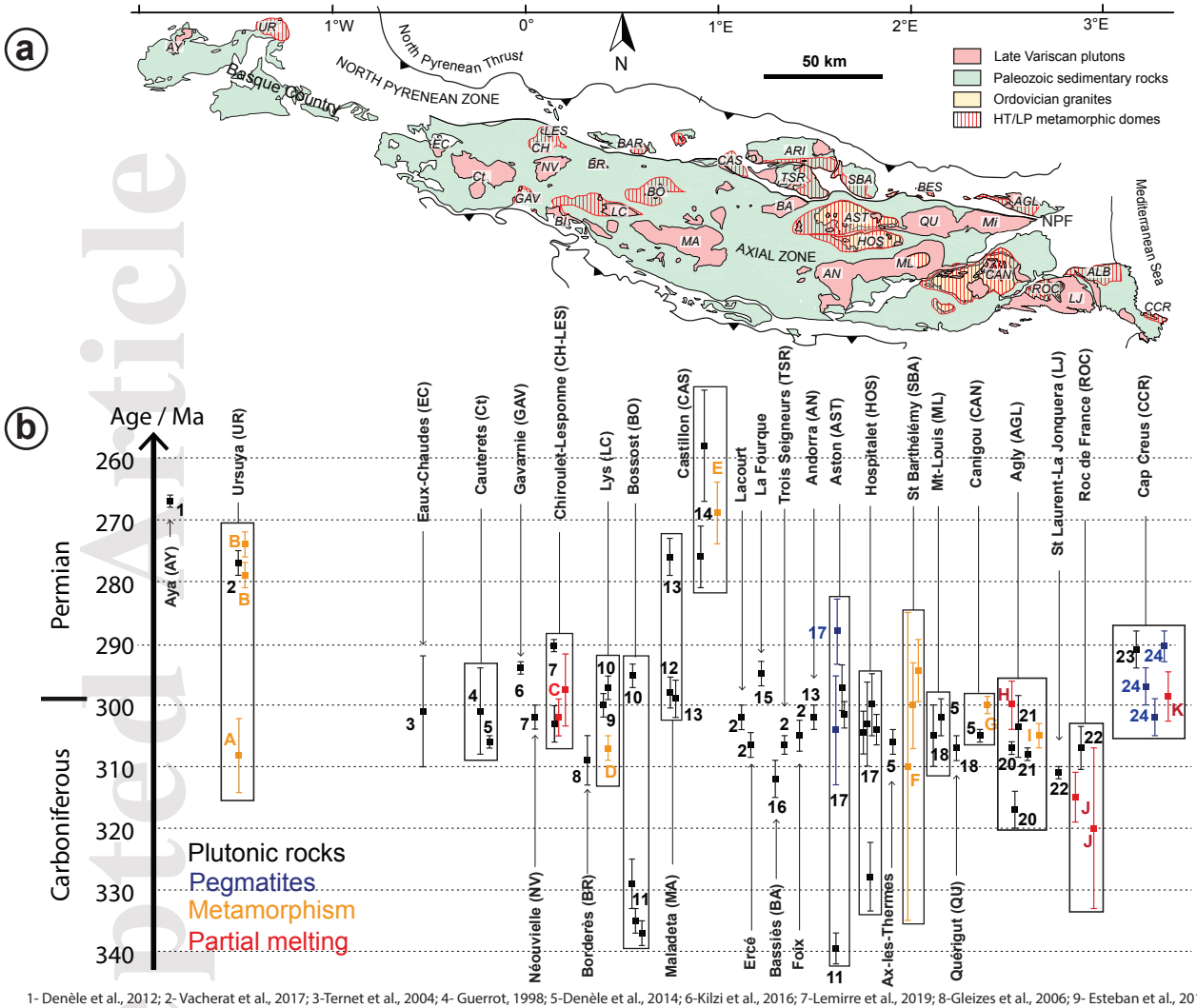

1- Denèle et al., 2012; 2- Vacherat et al., 2017; 3-Ternet et al., 2004; 4- Guerrot, 1998; 5-Denèle et al., 2014; 6-Kilzi et al., 2016; 7-Lemirre et al., 2019; 8-Gleizes et al., 2006; 9- Esteban et al., 2015; 10-Lopez-Sanchez et al., 2018; 11- Mezger and Gerdès, 2016; 12-Evans, 1993; 13- Pereira et al., 2014; 14-Kilzi, 2014; 15-Poitrenaud et al., 2019; 16-Paquette et al., 1997; 17- Schnapperelle et al., 2020; 18-Maurel et al., 2004; 19-Roberts et al., 2000; 20-Olivier et al., 2004; 21-Olivier et al., 2008; 22- Aguilar et al., 2014; 23-Druguet et al., 2014; 24- Van Lichtervelde et al., 2017.
A-Vacherat et al., 2017; B-Hart et al., 2016; C-Lemirre et al., 2019; D-Esteban et al., 2015; E-Kilzi, 2014; F-Delaperriere et al., 1994; G-de Hoÿm de Marien et al., 2019; H-Tournaire Guille et al., 2019; I- Siron et al., 2020; J-Aguilar et al., 2014; K- Druguet et al., 2014.

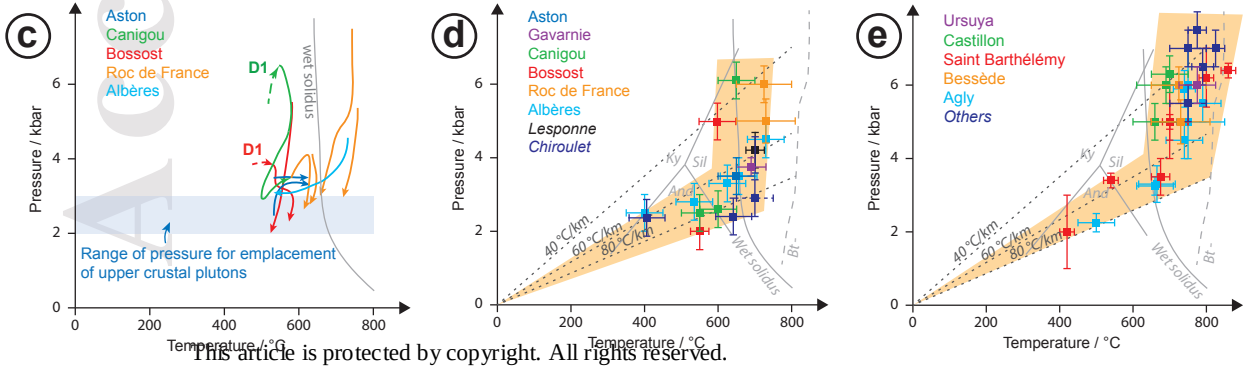

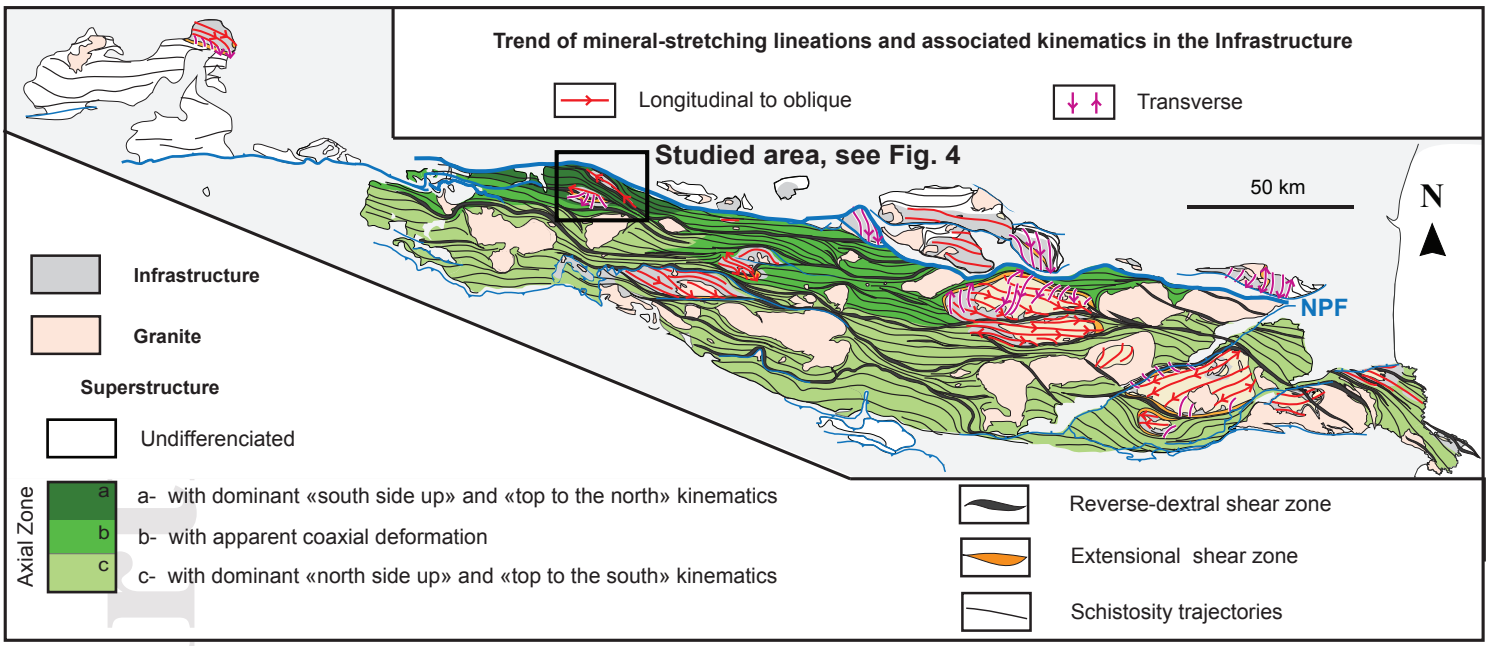

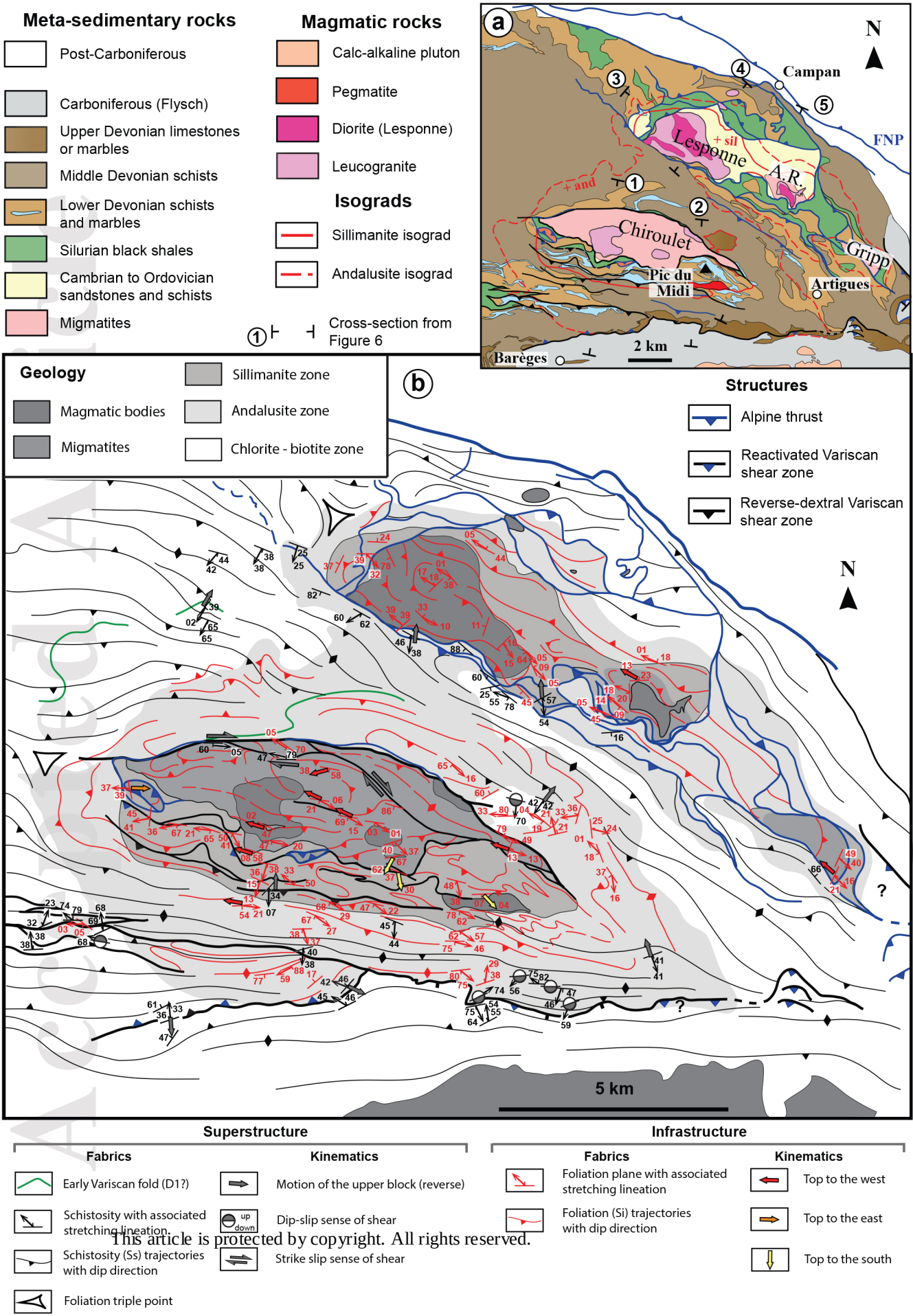

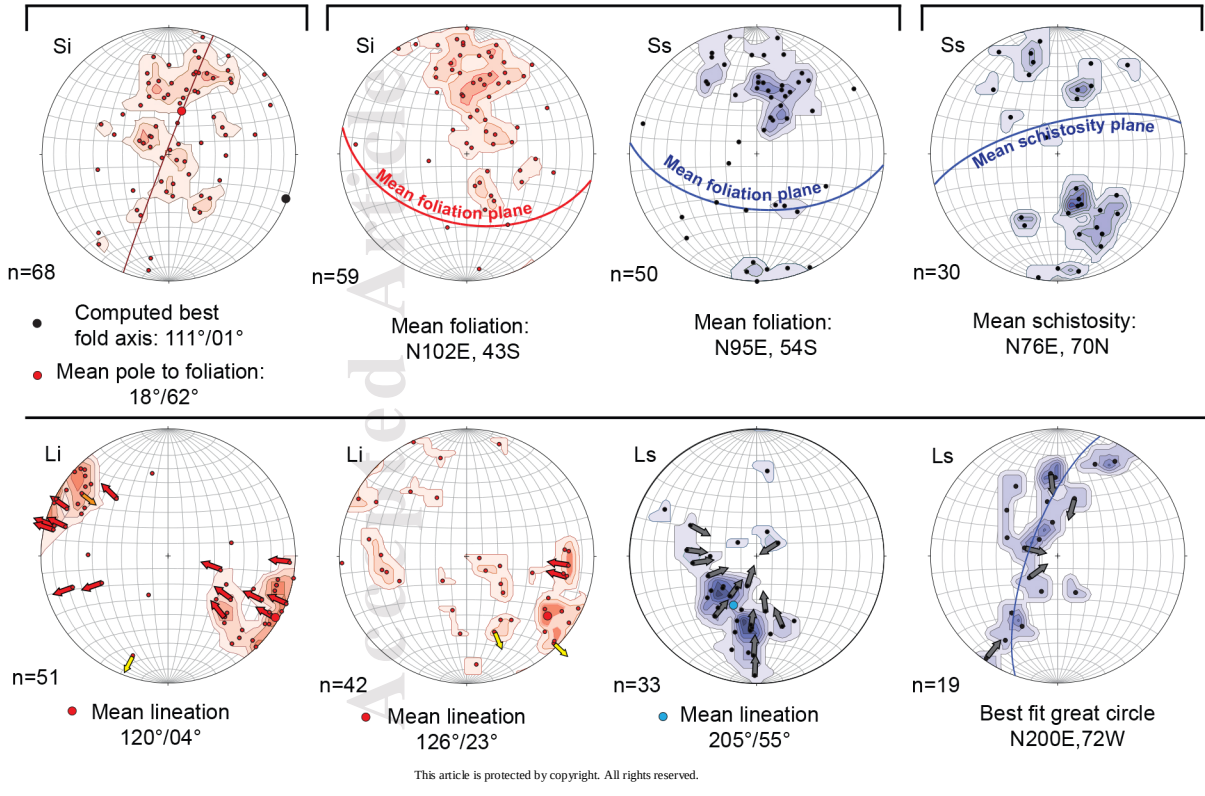

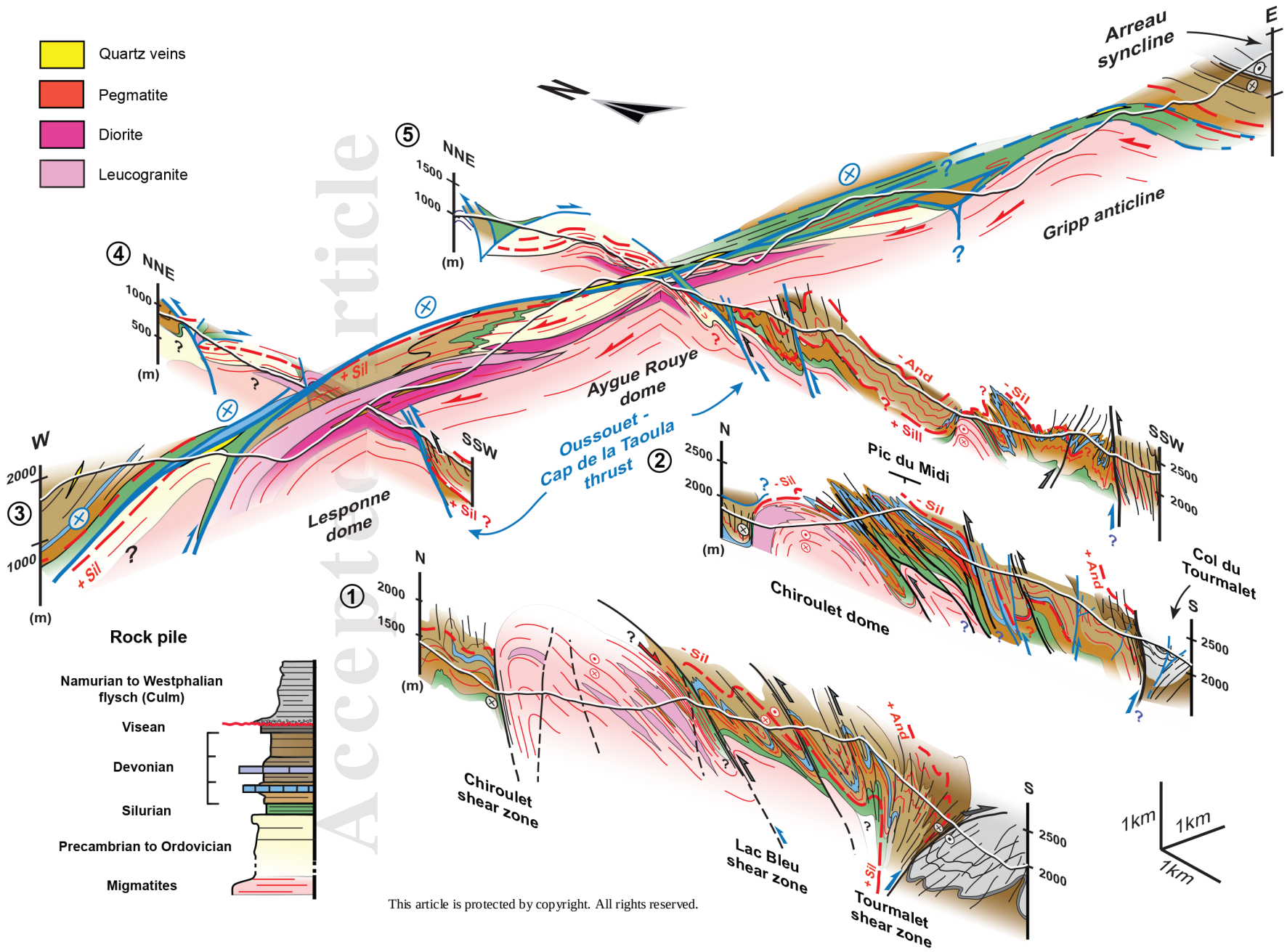
Quartz veins
Pegmatite
Diorite
Leucogranite
Arreau syncline
E
Gripp anticline
Aygue Rouye dome
Oussouet - Cap de la Taoula thrust
Lesponne dome
Pic du Midi
Chiroulet dome
Col du Tourmalet
Chiroulet shear zone
Lac Bleu shear zone
Tourmalet shear zone
Rock pile
Namurian to Westphalian flysch (Culm)
Visean
Devonian
Silurian
Precambrian to Ordovician
Migmatites
1km
1km
1km
This article is protected by copyright. All rights reserved.

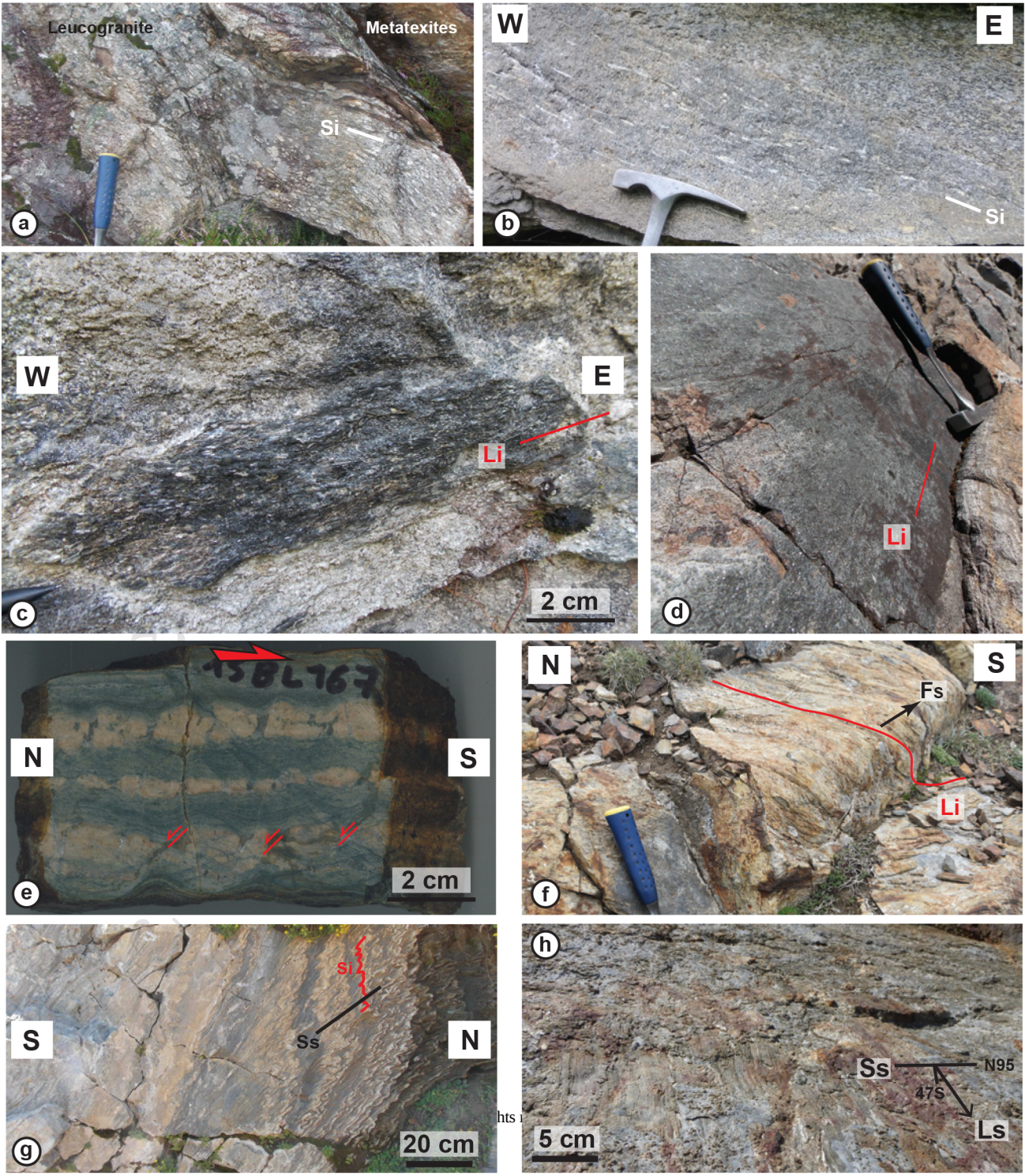
Leucogranite
Metatexites
Si
a
W
E
Si
b
W
E
Li
2 cm
c
Li
d
N
S
2 cm
e
N
S
Fs
Li
f
S
N
Si
Ss
20 cm
g
h
Ss
N95
47S
Ls
5 cm

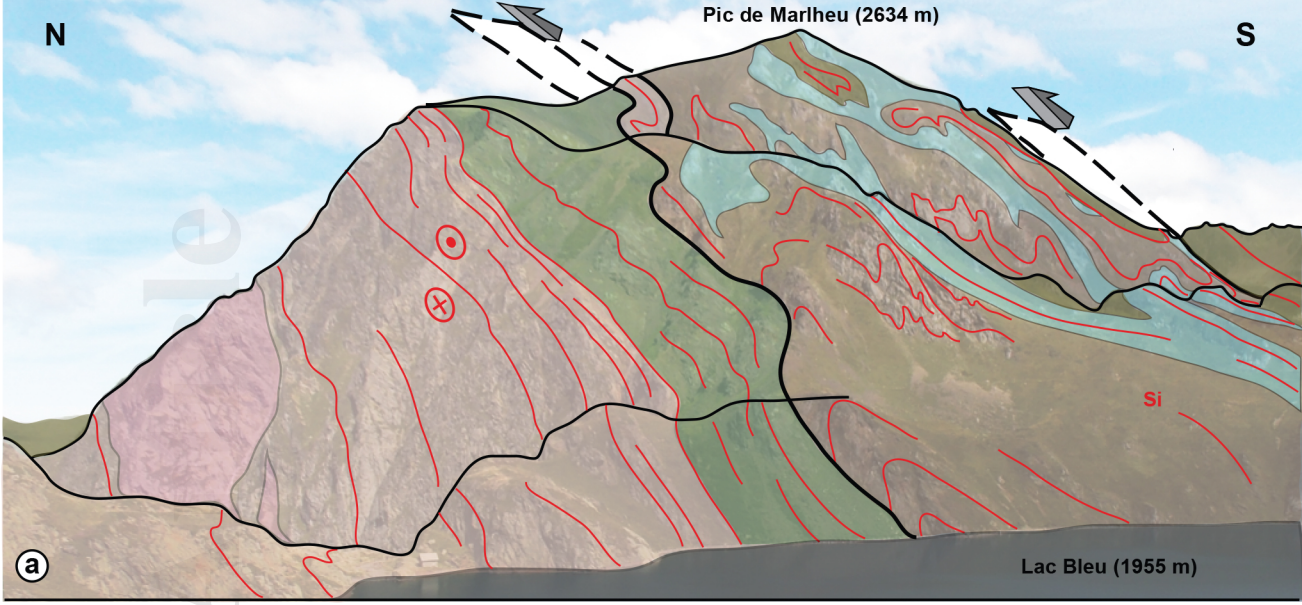

Schists (Middle Devonian)

Marble-sandstone alternations (Lower Devonian)

Migmatites

Marble (Lower Devonian)

Dark schists and paragneiss (Silurian)

Leucogranite

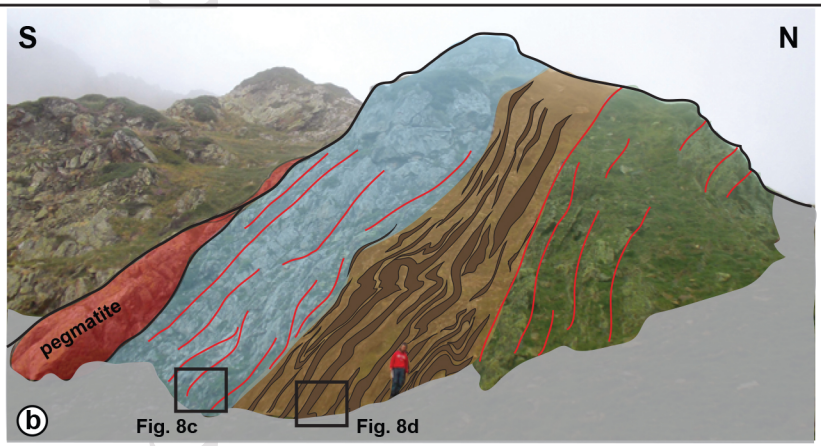

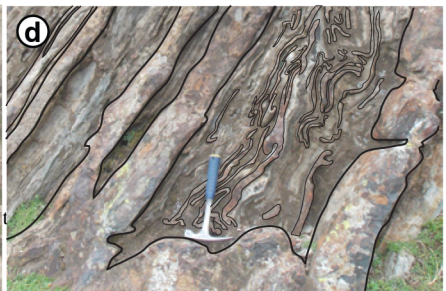

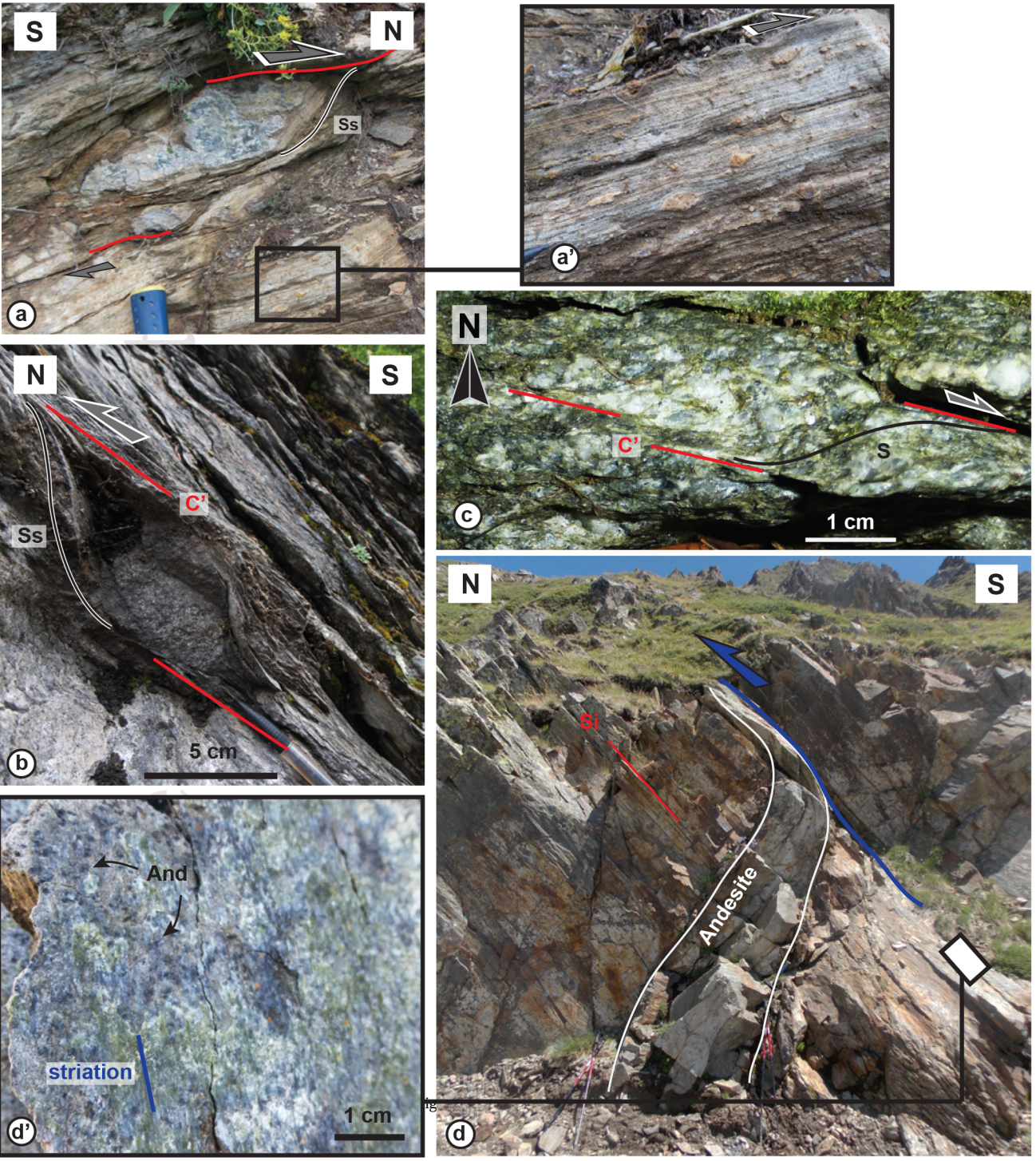
S
N
Ss
a
a'
N
S
C'
Ss
b
5 cm
N
C'
S
c
1 cm
N
S
Si
Andesite
d
And
striation
d'
1 cm

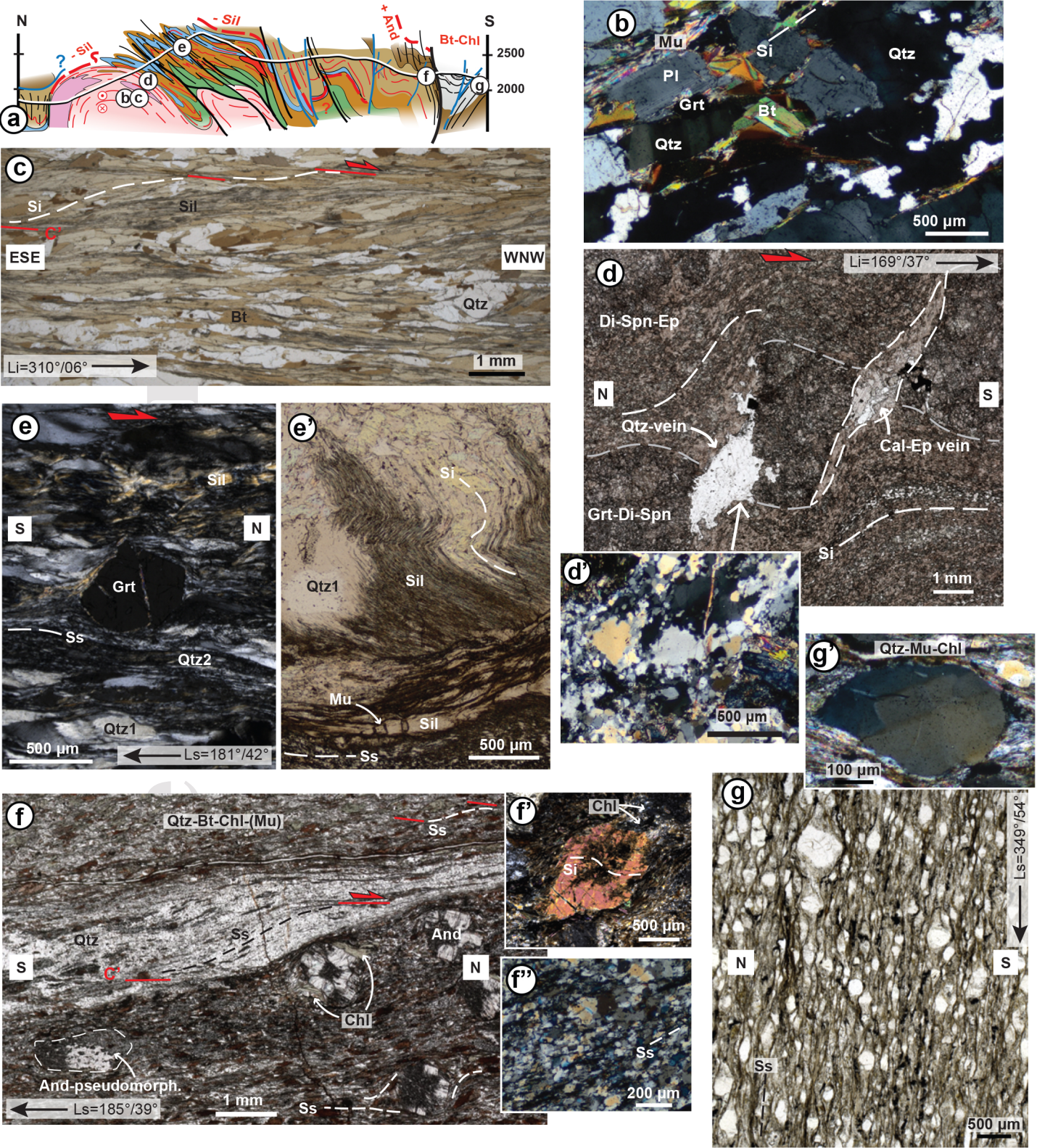
a
N
S
- Sil
+ And
Bt-Chl
2500
2000
? - Sil
e
d
b c
f
g
b
Mu
Si
Qtz
Pl
Grt
Bt
Qtz
500 µm
c
Si
Sil
C'
ESE
WNW
Qtz
Bt
Li=310°/06°
1 mm
d
Li=169°/37°
Di-Spn-Ep
N
S
Qtz-vein
Cal-Ep vein
Grt-Di-Spn
Si
1 mm
d'
500 µm
e
Sil
S
N
Grt
Ss
Qtz2
Qtz1
500 µm
Ls=181°/42°
e'
Si
Qtz1
Sil
Mu
Sil
Ss
500 µm
g'
Qtz-Mu-Chl
100 µm
f
Qtz-Bt-Chl-(Mu)
Ss
Qtz
Ss
And
S
C'
N
Chl
And-pseudomorph.
Ls=185°/39°
1 mm
Ss
f'
Chl
Si
500 µm
f''
Ss
200 µm
g
Ls=349°/54°
N
S
Ss
500 µm